

1 **Zn²⁺ is Essential for Ca²⁺ Oscillations in Mouse Eggs**

2

3 Hiroki Akizawa¹, Emily Lopes^{1,2}, Rafael A. Fissore^{1*}

4

5 ¹Department of Veterinary and Animal Sciences, University of Massachusetts Amherst,
6 661 North Pleasant Street, Amherst, Massachusetts, 01003, United States.

7 ²Molecular and Cellular Biology Graduate Program, University of Massachusetts,
8 Amherst, Massachusetts, 01003, United States.

9

10 **Running Title:** Labile Zn²⁺ and Ca²⁺ release

11

12 **Key Words:** Fertilization, mammals, Ca²⁺, IP₃R1, oocytes, eggs, sperm, divalent cations, chelators

13

14 *Author for correspondence (rfissore@umass.edu)

15

16 *Rafael A. Fissore

17 661 North Pleasant Street

18 ISB-427A

19 Department of Veterinary and Animal Science

20 University of Massachusetts, Amherst, 01003

21 Phone:413-687-5773

22 Email: rfissore@umass.edu

23

24 **Abstract**

25 Changes in the intracellular concentration of free calcium (Ca^{2+}) underpin egg
26 activation and initiation of development in animals and plants. In mammals, the Ca^{2+}
27 release is periodical, known as Ca^{2+} oscillations, and mediated by the type 1 inositol 1,4,5-
28 trisphosphate receptor ($\text{IP}_3\text{R1}$). Another divalent cation, zinc (Zn^{2+}), increases
29 exponentially during oocyte maturation and is vital for meiotic transitions, arrests, and
30 polyspermy prevention. It is unknown if these pivotal cations interplay during fertilization.
31 Here, using mouse eggs, we showed that basal concentrations of labile Zn^{2+} are
32 indispensable for sperm-initiated Ca^{2+} oscillations because Zn^{2+} -deficient conditions
33 induced by cell-permeable chelators abrogated Ca^{2+} responses evoked by fertilization and
34 other physiological and pharmacological agonists. We also found that chemically- or
35 genetically generated Zn^{2+} -deficient eggs displayed reduced $\text{IP}_3\text{R1}$ sensitivity and
36 diminished ER Ca^{2+} leak despite the stable content of the stores and $\text{IP}_3\text{R1}$ mass.
37 Resupplying Zn^{2+} restarted Ca^{2+} oscillations, but excessive Zn^{2+} prevented and terminated
38 them, hindering $\text{IP}_3\text{R1}$ responsiveness. The findings suggest that a permissive window of
39 Zn^{2+} concentrations is required for Ca^{2+} responses and $\text{IP}_3\text{R1}$ function in eggs, ensuring
40 optimal response to fertilization and egg activation.

41

42 **Introduction**

43 Vertebrate eggs are arrested at the metaphase stage of the second meiosis (MII)
44 when ovulated because they have an active Cdk1/cyclin B complex and inactive
45 APC/C^{Cdc20} (Heim et al., 2018). Release from MII initiates egg activation, the first
46 hallmark of embryonic development (Ducibella et al., 2002; Schultz and Kopf, 1995).
47 The universal signal of egg activation is an increase in the intracellular concentration of
48 calcium (Ca^{2+}) (Ridgway et al., 1977; Stricker, 1999). Ca^{2+} release causes the inactivation
49 of the APC/C inhibitor Emi2, which enhances cyclin B degradation and induces meiotic
50 exit (Lorca et al., 1993; Shoji et al., 2006; Suzuki et al., 2010a). In mammals, the
51 stereotypical fertilization Ca^{2+} signal, oscillations, consists of transient but periodical
52 Ca^{2+} increases that promote progression into interphase (Deguchi et al., 2000; Miyazaki
53 et al., 1986). The sperm-borne Phospholipase C zeta1 ($\text{PLC}\zeta$) persistently stimulates the
54 production of inositol 1,4,5-trisphosphate (IP_3) (Matsu-ura et al., 2019; Saunders et al.,
55 2002; Wu et al., 2001) that binds its cognate receptor in the endoplasmic reticulum (ER),
56 $\text{IP}_3\text{R1}$ and causes Ca^{2+} release from the egg's main Ca^{2+} reservoir (Wakai et al., 2019).
57 The intake of extracellular Ca^{2+} via plasma membrane channels and transporters ensures
58 the persistence of the oscillations (Miao et al., 2012; Stein et al., 2020; Wakai et al., 2019,
59 2013).

60 Before fertilization, maturing oocytes undergo cellular and biochemical
61 modifications (see for review (Ajduk et al., 2008)). The nucleus of immature oocytes,
62 known as the germinal vesicle (GV), undergoes the breakdown of its envelope marking
63 the onset of maturation and setting in motion a series of cellular events that culminate
64 with the release of the first polar body, the correct ploidy for fertilization, and re-arrest at
65 MII (Eppig, 1996). Other organelles are also reorganized, such as cortical granules
66 migrate to the cortex for exocytosis and polyspermy block, mitochondria undergo
67 repositioning, and the cytoplasm's redox state becomes progressively reduced to promote
68 the exchange of the sperm's protamine load (Liu, 2011; Perreault et al., 1988; Wakai et
69 al., 2014). Wide-ranging adaptations also occur in the Ca^{2+} release machinery to produce
70 timely and protracted Ca^{2+} oscillations following sperm entry (Fujiwara et al., 1993;
71 Lawrence et al., 1998), including the increase in the content of the Ca^{2+} stores, ER
72 reorganization with cortical cluster formation, and increased IP₃R1 sensitivity (Lee et al.,
73 2006; Wakai et al., 2012). The total intracellular levels of zinc (Zn^{2+}) also remarkably
74 increase during maturation, amounting to a 50% rise, which is necessary for oocytes to
75 proceed to the telophase I of meiosis and beyond (Kim et al., 2010). Remarkably, after
76 fertilization, Zn^{2+} levels need to decrease, as Emi2 is a Zn^{2+} -associated molecule, and
77 high Zn^{2+} levels prevent MII exit (Bernhardt et al., 2012; Shoji et al., 2014; Suzuki et al.,
78 2010b). Following the initiation of Ca^{2+} oscillations, approximately 10 to 20% of the Zn^{2+}
79 accrued during maturation is ejected during the Zn^{2+} sparks, a conserved event in
80 vertebrates and invertebrate species (Kim et al., 2011; Que et al., 2019; Tokuhiko and
81 Dean, 2018; Wozniak et al., 2020; Zhang et al., 2016). The use of Zn^{2+} chelators such as
82 N,N,N,N-tetrakis (2-pyridinylmethyl)-1,2-ethylenediamine (TPEN) to create Zn^{2+} -
83 deficient conditions buttressed the importance of Zn^{2+} during meiotic transitions (Kim et
84 al., 2010; Suzuki et al., 2010b). However, whether the analogous dynamics of Ca^{2+} and
85 Zn^{2+} during maturation imply crosstalk and Zn^{2+} levels modulate Ca^{2+} release during
86 fertilization is unknown.

87 IP₃Rs are the most abundant intracellular Ca^{2+} release channel in non-muscle
88 cells (Berridge, 2016). They form a channel by assembling into tetramers with each
89 subunit of ~270kDa MW (Taylor and Tovey, 2010). Mammalian eggs express the type I
90 IP₃R, the most widespread isoform (Fissore et al., 1999; Parrington et al., 1998). IP₃R1 is
91 essential for egg activation because its inhibition precludes Ca^{2+} oscillations (Miyazaki
92 and Ito, 2006; Miyazaki et al., 1992; Xu et al., 2003). Myriad and occasionally cell-
93 specific factors influence Ca^{2+} release through the IP₃R1 (Taylor and Tovey, 2010). For
94 example, following fertilization, IP₃R1 undergoes ligand-induced degradation caused by
95 the sperm-initiated long-lasting production of IP₃ that effectively reduces the IP₃R1 mass

96 (Brind et al., 2000; Jellerette et al., 2000). Another regulatory mechanism is Ca^{2+} , a
97 universal cofactor, which biphasically regulates IP_3Rs ' channel opening (Iino, 1990; Jean
98 and Klee, 1986), congruent with several Ca^{2+} and calmodulin binding sites on the
99 channel's sequence (Sienaert et al., 1997; Sipma et al., 1999). Notably, Zn^{2+} may also
100 participate in $\text{IP}_3\text{R1}$ regulation. Recent studies using electron cryomicroscopy (cryoEM),
101 a technique that allows peering into the structure of $\text{IP}_3\text{R1}$ with a near-atomic resolution,
102 have revealed that a helical linker (LNK) domain near the C-terminus mediates the
103 coupling between the N- and C-terminal ends necessary for channel opening (Fan et al.,
104 2015). The LNK domain contains a putative Zinc-finger motif proposed to be vital for
105 $\text{IP}_3\text{R1}$ function (Fan et al., 2015; Paknejad and Hite, 2018). Therefore, the exponential
106 increase in Zn^{2+} levels in maturing oocytes, besides its essential role in meiosis
107 progression, may optimize the $\text{IP}_3\text{R1}$ function, revealing hitherto unknown cooperation
108 between these cations during fertilization.

109 Here, we examined whether crosstalk between Ca^{2+} and Zn^{2+} is required to
110 initiate and sustain Ca^{2+} oscillations and maintain Ca^{2+} store content in MII eggs. We
111 found that Zn^{2+} -deficient conditions inhibited Ca^{2+} release and oscillations without
112 reducing Ca^{2+} stores, IP_3 production, $\text{IP}_3\text{R1}$ expression, or altering the viability of eggs or
113 zygotes. We show instead that Zn^{2+} deficiency impaired $\text{IP}_3\text{R1}$ function and lessened the
114 receptor's ability to gate Ca^{2+} release out of the ER. Remarkably, resupplying Zn^{2+} re-
115 established the oscillations interrupted by low Zn^{2+} , although persistent increases in
116 intracellular Zn^{2+} were harmful, disrupting the Ca^{2+} responses and preventing egg
117 activation. Together, the results show that besides contributing to oocyte maturation, Zn^{2+}
118 has a central function in Ca^{2+} homeostasis such that optimal Zn^{2+} concentrations ensure
119 $\text{IP}_3\text{R1}$ function and the Ca^{2+} oscillations required for initiating embryo development.

120

121 **Results**

122 ***TPEN dose-dependently lowers intracellular Zn^{2+} and inhibits sperm-initiated Ca^{2+}***
123 ***oscillations.***

124 TPEN is a cell-permeable, non-specific chelator with a high affinity for transition
125 metals widely used to study their function in cell physiology (Arslan et al., 1985; Lo et
126 al., 2020). Mouse oocytes and eggs have exceedingly high intracellular concentrations of
127 Zn^{2+} (Kim et al., 2011, 2010), and the TPEN-induced defects in the progression of meiosis
128 have been ascribed to its chelation (Bernhardt et al., 2011; Kim et al., 2010). In support
129 of this view, the Zn^{2+} levels of cells showed acute reduction after TPEN addition, as
130 reported by indicators such as FluoZin-3 (Arslan et al., 1985; Suzuki et al., 2010b).
131 Studies in mouse eggs also showed that the addition of μM concentrations of TPEN

132 disrupted Ca^{2+} oscillations initiated by fertilization or SrCl_2 (Lawrence et al., 1998;
133 Suzuki et al., 2010b), but the mechanism(s) and target(s) of the inhibition remained
134 unknown. To gain insight into this phenomenon, we first performed dose-titration studies
135 to determine the effectiveness of TPEN in lowering Zn^{2+} in eggs. The addition of 2.5 μM
136 TPEN protractedly reduced Zn^{2+} levels, whereas 5 and 10 μM TPEN acutely and
137 persistently reduced FluoZin-3 fluorescence (**Fig. 1A**). These concentrations of TPEN are
138 higher than the reported free Zn^{2+} concentrations in cells, but within range of those of
139 found in typical culture conditions (Lo et al., 2020; Qin et al., 2011). We next determined
140 the concentrations of TPEN required to abrogate fertilization-initiated oscillations.
141 Following intracytoplasmic sperm injection (ICSI), we monitored Ca^{2+} responses while
142 increasing TPEN concentrations. As shown in **Fig. 1B**, 5 and 10 μM TPEN effectively
143 blocked ICSI-induced Ca^{2+} oscillations in over half of the treated cells, and the remaining
144 eggs, after a prolonged interval, resumed lower-frequency rises (**Fig. 1B-center panels**).
145 Finally, 50 μM or greater concentrations of TPEN permanently blocked these oscillations
146 (**Fig. 1B-right panel**). It is noteworthy that at the time of addition, TPEN induces a sharp
147 drop in basal Fura-2 F340/ F380 ratios, consistent with Fura-2's high affinity for Zn^{2+}
148 (Snitsarev et al., 1996).

149 We next used membrane-permeable and -impermeable chelators to assess
150 whether TPEN inhibited Ca^{2+} oscillations by chelating Zn^{2+} from intracellular or
151 extracellular compartments. The addition of the high-affinity but cell-impermeable Zn^{2+}
152 chelators DTPA and EDTA neither terminated nor temporarily interrupted ICSI-induced
153 Ca^{2+} oscillations (**Fig. 1C**). Protractedly, Ca^{2+} oscillations slowed down, possibly because
154 of chelation and lowering of external Ca^{2+} (**Fig. 1C**). Conversely, TPA, a permeable Zn^{2+}
155 chelator, blocked the ICSI-initiated oscillations but required higher concentrations than
156 TPEN (**Fig. 1D**). Collectively, the data suggest that basal levels of labile Zn^{2+} are essential
157 to sustain the fertilization-initiated Ca^{2+} oscillations in eggs.

158 We next evaluated whether TPEN supplementation prevented the completion of
159 meiosis and pronuclear (PN) formation following fertilization (**Fig. 1E and Table 1**). All
160 fertilized eggs promptly extruded second polar bodies regardless of treatment (**Fig. 1E**).
161 TPEN, however, impaired PN formation, and by 4- or 7-hr. post-ICSI, most treated eggs
162 failed to show PNs, unlike controls (**Fig. 1E and Table 1**). Together, these results
163 demonstrate that depletion of Zn^{2+} terminates Ca^{2+} oscillations and delays or prevents
164 events of egg activation, including PN formation.

165

166 ***TPEN is a universal inhibitor of Ca^{2+} oscillations in eggs.***

167 Mammalian eggs initiate Ca^{2+} oscillations in response to numerous stimuli and

168 conditions (Miyazaki and Ito, 2006; Wakai and Fissore, 2013). Fertilization and its release
169 of PLC ζ stimulate the phosphoinositide pathway leading to the production of IP $_3$ and Ca $^{2+}$
170 oscillations (Miyazaki, 1988; Saunders et al., 2002). Neurotransmitters such as
171 acetylcholine (Ach) and other G-protein coupled receptor agonists engage a similar
172 mechanism (Dupont et al., 1996; Kang et al., 2003), although in these cases, IP $_3$
173 production occurs at the plasma membrane and is short-lived (Kang et al., 2003; Swann
174 and Parrington, 1999). Agonists such as SrCl $_2$ and thimerosal generate oscillations by
175 sensitizing IP $_3$ R1 without producing IP $_3$. The mechanism(s) of SrCl $_2$ is unclear, although
176 its actions are reportedly directly on the IP $_3$ R1 (Hajnóczky and Thomas, 1997; Hamada
177 et al., 2003; Nomikos et al., 2015, 2011; Sanders et al., 2018). Thimerosal oxidizes dozens
178 of thiol groups in the receptor, which enhances the receptor's sensitivity and ability to
179 release Ca $^{2+}$ (Bootman et al., 1992; Evellin et al., 2002; Joseph et al., 2018). We took
180 advantage of the varied points at which the mentioned agonists engage the
181 phosphoinositide pathway to examine TPEN's effectiveness in inhibiting their effects.
182 *mPlcz* mRNA injection, like fertilization, induces persistent Ca $^{2+}$ oscillations, although
183 *mPlcz*'s tends to be more robust. Consistent with this, the addition of 10 and 25 μ M TPEN
184 transiently interrupted or belatedly terminated oscillations, whereas 50 μ M acutely
185 stopped all responses (**Fig. 2A**). By contrast, SrCl $_2$ -initiated rises were the most sensitive
186 to Zn $^{2+}$ -deficient conditions, with 2.5 μ M TPEN nearly terminating all oscillations that 5
187 μ M did (**Fig. 2B**). TPEN was equally effective in ending the Ach-induced Ca $^{2+}$ responses
188 (**Fig. 2C**), but curbing thimerosal responses required higher concentrations (**Fig. 2D**).
189 Lastly, we ruled out that downregulation of IP $_3$ R1 was responsible for the slow-down or
190 termination of the oscillations by TPEN. To accomplish this, we examined the IP $_3$ R1 mass
191 in eggs (Jellerette et al., 2004) with and without TPEN supplementation and injection of
192 *mPlcz* mRNA. By 4-h post-injection, the mRNA induced the expected down-regulation
193 of IP $_3$ R1 reactivity vs. uninjected eggs, but in TPEN-treated and *Plcz* mRNA-injected
194 eggs, the decrease was insignificant (**Fig. 2F**). These findings together show that Zn $^{2+}$
195 deficiency inhibits the IP $_3$ R1-mediated Ca $^{2+}$ oscillations independently of IP $_3$ production
196 or loss of receptor, suggesting a role of Zn $^{2+}$ on IP $_3$ R1 function (**Fig. 2E**).

197

198 ***Zn $^{2+}$ depletion reduces IP $_3$ R1-mediated Ca $^{2+}$ release.***

199 To directly assess the inhibitory effects of TPEN on IP $_3$ R1 function, we used caged
200 IP $_3$ (cIP $_3$) that, after short UV pulses, releases IP $_3$ into the ooplasm (Wakai et al., 2012;
201 Walker et al., 1987). To exclude the possible contribution of external Ca $^{2+}$ to the responses,
202 we performed the experiments in Ca $^{2+}$ -free media. In response to sequential cIP $_3$ release
203 5 min. apart, control eggs displayed corresponding Ca $^{2+}$ rises that occasionally

204 transitioned into short-lived oscillations (**Fig. 3A**). The addition of TPEN after the third
205 cIP₃ release prevented the subsequent Ca²⁺ response and prematurely terminated the in-
206 progress Ca²⁺ rises (**Fig. 3B and inset**). Pre-incubation of eggs with TPEN precluded
207 cIP₃-induced Ca²⁺ release, even after 5 sec. of UV exposure (**Fig. 3C**). The addition of
208 excess ZnSO₄ (100 μM) overcame TPEN's inhibitory effects, but only if added before
209 (**Fig. 3E**) and not after the addition of TPEN (**Fig. 3D**). Similar concentrations of MgCl₂
210 or CaCl₂ failed to reverse TPEN effects (**Fig. 3F, G**). Together, the results show that Zn²⁺
211 is required for IP₃R1-mediated Ca²⁺ release downstream of IP₃ production, appearing to
212 interfere with receptor gating, as suggested by TPEN's rapid termination of in-progress
213 Ca²⁺ rises and ongoing oscillations.

214 ERp44 is an ER luminal protein of the thioredoxin family that interacts with the
215 IP₃R1, reportedly inhibiting its ability to mediate Ca²⁺ release (Higo et al., 2005). The
216 localization of ERp44 in the ER-Golgi intermediate compartment of somatic cells
217 correlates with Zn²⁺'s availability and changes dramatically after TPEN treatment (Higo
218 et al., 2005; Watanabe et al., 2019). To rule out the possibility that TPEN suppresses the
219 function of IP₃R1 by modifying the subcellular distribution of ERp44, we overexpressed
220 ERp44 by injecting HA tagged-*Erp44* mRNA into MII eggs and monitored the effect on
221 Ca²⁺ release. TPEN did not alter the localization of ERp44 (**Supplementary Fig. 1A**),
222 and overexpression of ERp44 modified neither the Ca²⁺ oscillations induced by agonists
223 (**Supplementary Fig. 1B**) nor the effectiveness of TPEN to block them (data not shown).
224 Thus, TPEN and Zn²⁺ deficiency most likely inhibits Ca²⁺ release by directly interfering
225 with IP₃R1 function rather than modifying this particular regulator.

226

227 ***Zn²⁺ depletion diminishes the ER Ca²⁺ leak and increases Ca²⁺ store content.***

228 Our above cIP₃ results that TPEN inhibited IP₃R1-mediated Ca²⁺ release and
229 interrupted in-progress Ca²⁺ rises despite the presence of high levels of environmental IP₃
230 suggest its actions are probably independent of IP₃ binding, agreeing with an earlier report
231 showing that TPEN did not modify IP₃'s affinity for the IP₃R (Richardson and Taylor,
232 1993). Additionally, the presence of a Zn²⁺-binding motif near the C-term cytoplasmic
233 domain of the IP₃R1's channel, which is known to influence agonist-induced IP₃R1 gating
234 (Fan et al., 2015), led us to posit and examine that Zn²⁺ deficiency may be disturbing Ca²⁺
235 release to the cytosol and out of the ER. To probe this possibility, we queried if pre-
236 treatment with TPEN inhibited Ca²⁺ release through IP₃R1. We first used Thapsigargin
237 (Tg), a Sarcoplasmic/ER Ca²⁺ ATPase pump inhibitor (Thastrup et al., 1990) that unmasks
238 a constitutive Ca²⁺ leak out of the ER (Lemos et al., 2021); in eggs, we have demonstrated
239 it is mediated at least in part by IP₃R1 (Wakai et al., 2019). Treatment with TPEN for 15

240 min. slowed the Tg-induced Ca^{2+} leak into the cytosol, resulting in delayed and lowered
241 amplitude Ca^{2+} responses (**Fig. 4A**; $P < 0.05$). To test whether the reduced response to Tg
242 means that TPEN left a temporarily increased Ca^{2+} content in the ER after it, we added
243 the Ca^{2+} ionophore ionomycin (Io), which empties all stores independently of IP_3Rs . Io-
244 induced Ca^{2+} responses were 3.3-fold greater in TPEN-treated cells, supporting the view
245 that TPEN interferes with the ER Ca^{2+} leak (**Fig. 4A**; $P < 0.05$). We further evaluated this
246 concept using *in vitro* aged eggs that often display reduced Ca^{2+} store content than freshly
247 collected counterparts (Abbott et al., 1998). After culturing eggs in the presence or
248 absence of TPEN for 2-hr., we added Io during Ca^{2+} monitoring, which in TPEN-treated
249 eggs induced bigger Ca^{2+} rises than in control eggs (**Fig. 4B**; $P < 0.05$). We confirmed that
250 this effect was independent of $\text{IP}_3\text{R1}$ degradation because TPEN did not change $\text{IP}_3\text{R1}$
251 reactivity in unfertilized eggs (**Fig. 4C**; $P < 0.05$).

252 Next, we used the genetically encoded FRET sensor D1ER (Palmer et al., 2004) to
253 assess the TPEN's effect on the ER's relative Ca^{2+} levels changes following the additions
254 of Tg or Ach. TPEN was added 10 min. before 10 μM Tg or 50 μM Ach, and we
255 simultaneously monitored changes in cytosolic and intra-ER Ca^{2+} (**Fig. 4D, E**). For the
256 first three min., the Tg-induced decrease in Ca^{2+} -ER was similar between groups.
257 However, while the drop in Ca^{2+} content continued in control eggs, in TPEN-treated eggs,
258 it came to an abrupt halt, generating profound differences between the two groups (**Fig.**
259 **4D**; $P < 0.05$). TPEN had even more pronounced effects following the addition of Ach,
260 leading to a reduced- and prematurely terminated- Ca^{2+} release from the ER in treated
261 eggs (**Fig. 4E**; $P < 0.05$).

262 Lastly, we sought to use a cellular model where low labile Zn^{2+} occurred without
263 pharmacology. To this end, we examined a genetic model where the two non-selective
264 plasma membrane channels that could influx Zn^{2+} in maturing oocytes have been deleted
265 (Bernhardt et al., 2017; Carvacho et al., 2016, 2013), namely, the transient receptor
266 potential melastatin-7 (TRPM7) and TRP vanilloid 3 (TRPV3), both members of the TRP
267 superfamily of channels (Wu et al., 2010). We found that eggs from double knockout
268 females (dKOs) had lower labile Zn^{2+} levels (**Fig. 4F**), and the addition of Tg revealed an
269 expanded Ca^{2+} store content in these eggs vs. control WT eggs (**Fig. 4G**). Remarkably, in
270 dKO eggs, the Ca^{2+} rise induced by Tg showed a shoulder or inflection point before the
271 peak delaying the time to peak (**Fig. 4G, inset**; $P < 0.001$). These results in dKO eggs
272 show a changed dynamic of the Tg-induced Ca^{2+} release, suggesting that Zn^{2+} deficient
273 levels modify ER Ca^{2+} release independently of chelators.

274

275 ***Ca^{2+} oscillations in eggs occur within a window of Zn^{2+} concentrations.***

276 We next examined if resupplying Zn^{2+} could restart the Ca^{2+} oscillations
277 terminated by Zn^{2+} depletion. Zn pyrithione (ZnPT) rapidly increases cellular Zn^{2+} upon
278 extracellular addition (Barnett et al., 1977; Robinson, 1964). Dose titration studies and
279 imaging fluorimetry revealed that 0.01 μM ZnPT caused subtle and protracted increases
280 in Zn^{2+} levels, whereas 0.1 μM ZnPT caused rapid increases in eggs' Zn^{2+} baseline (**Fig.**
281 **5A**). We induced detectable Ca^{2+} oscillations by injection of *mPlcz* mRNA followed by
282 50 μM TPEN (**Fig. 5B**), which terminated them. After 30 min, we added 0.1 μM ZnPT,
283 and within 15 min. the oscillations restarted in most TPEN-treated eggs (**Fig. 5C**). We
284 repeated this approach using Thimerosal (**Fig. 5D, E**). Adding 0.1 μM ZnPT did not
285 restore the Ca^{2+} oscillations retrained by TPEN, but 0.5 μM ZnPT did so (**Fig. 5E**). These
286 results demonstrate that Zn^{2+} plays a pivotal, enabling role in the generation of Ca^{2+}
287 oscillations in mouse eggs.

288

289 ***Excessive intracellular Zn^{2+} inhibits Ca^{2+} oscillations.***

290 Zn^{2+} is necessary for diverse cellular functions, consistent with numerous amino
291 acids and proteins capable of binding Zn^{2+} within specific and physiological ranges (Pace
292 and Weerapana, 2014). Excessive Zn^{2+} , however, can cause detrimental effects on cells
293 and organisms (Broun et al., 1990; Hara et al., 2022; Sikora and Ouagazzal, 2021).
294 Consistent with the deleterious effects of Zn^{2+} , a previous study showed that high
295 concentrations of ZnPT, $\sim 50 \mu M$, prevented $SrCl_2$ -induced egg activation and initiation
296 of development (Bernhardt et al., 2012; Kim et al., 2011). We examined how ZnPT and
297 excessive Zn^{2+} levels influence Ca^{2+} oscillations. Our conditions revealed that pre-
298 incubation or continuous exposure to 0.1 μM or 1.0 μM ZnPT delayed or prevented egg
299 activation induced by *mPlcz* mRNA injection (**Supplementary Fig. 2**). We used these
300 ZnPT concentrations to add it into ongoing oscillations induced by ICSI and monitored
301 the succeeding Ca^{2+} responses. The addition of 0.05 to 10 μM ZnPT caused an immediate
302 elevation of the basal levels of Fura-2 and termination of the Ca^{2+} oscillations (**Fig. 6A-**
303 **D**). *mPlcz* mRNA-initiated Ca^{2+} responses were also interrupted by adding 0.1 μM ZnPT,
304 whereas untreated eggs continued oscillating (**Fig. 6E, F**). ZnPT also inhibited IP_3R1 -
305 mediated Ca^{2+} release triggered by cIP_3 , suggesting that excessive Zn^{2+} directly inhibits
306 IP_3R1 function (**Fig. 6G**).

307 The increased basal ratios of Fura-2 caused by the addition of ZnPT are unlikely
308 to represent changes in basal Ca^{2+} levels because they would have likely caused some
309 cellular responses such as the release of the second polar body, egg fragmentation, or cell
310 death, neither of which happened. It might reflect, instead, Fura-2's ability to report
311 changes in Zn^{2+} levels, which was the case because the addition of TPEN lowered the

312 Fura-2 ratios without restarting the Ca^{2+} oscillations (**Fig. 6F**). To ensure the impact of
313 ZnPT abolishing Ca^{2+} oscillations was not an imaging artifact obscuring ongoing rises,
314 we simultaneously monitored cytoplasmic and ER Ca^{2+} levels with Rhod-2 and D1ER,
315 respectively. This approach allowed synchronously observing opposite Ca^{2+} changes in
316 the two compartments. In uninjected eggs, the fluorescent values remained unchanged,
317 and in *mPlcz* mRNA-injected eggs, the reporters' signals displayed the expected opposite
318 changes (**Fig. 6H, I**). The addition of ZnPT rapidly increased Rhod-2 signals in uninjected
319 and oscillating eggs, unlike D1ER's, suggesting it cannot detect changes in Zn^{2+} levels to
320 this extent despite faithfully reporting Ca^{2+} changes. In oscillating eggs following ZnPT
321 addition, D1ER progressively showed fewer and lower amplitude changes, consistent
322 with the diminishing and eventual termination of the Ca^{2+} oscillations. Noteworthy, the
323 basal fluorescent ratio of D1ER in these eggs remained unchanged after ZnPT, further
324 demonstrating its unresponsiveness to Zn^{2+} changes of this magnitude. We confirmed that
325 both reporters were still in working order, as the addition of Io triggered Ca^{2+} changes
326 detected by both reporters (**Fig. 6H, I**).

327

328 **Discussion**

329 The present study demonstrates that appropriate levels of labile Zn^{2+} are essential
330 for initiating and maintaining $\text{IP}_3\text{R1}$ -mediated Ca^{2+} oscillations in mouse eggs regardless
331 of the initiating stimuli. Both deficient and excessive Zn^{2+} compromise $\text{IP}_3\text{R1}$ sensitivity,
332 diminishing and mostly terminating Ca^{2+} oscillations. The results demonstrate that $\text{IP}_3\text{R1}$
333 and Zn^{2+} act in concert to modulate Ca^{2+} signals revealing previously unexplored
334 crosstalk between these ions at fertilization (**Fig. 7**).

335 Zn^{2+} is an essential micronutrient for living organisms (Kaur et al., 2014) and is
336 required for various cellular functions, such as proliferation, transcription, and
337 metabolism (Lo et al., 2020; Maret and Li, 2009; Yamasaki et al., 2007). Studies using
338 Zn^{2+} chelators have uncovered what appears to be a cell-specific, narrow window of Zn^{2+}
339 concentrations needed for cellular proliferation and survival (Carraway and Dobner,
340 2012; Lo et al., 2020). Further, TPEN appeared especially harmful, and in a few cell lines,
341 even low doses provoked oxidative stress, DNA fragmentation, and apoptosis (Mendivil-
342 Perez et al., 2012). We show here that none of the Zn^{2+} chelators, permeable or
343 impermeable, affected cell viability within our experimental observations, confirming
344 findings from previous studies that employed high concentrations of TPEN to interrupt
345 the Ca^{2+} oscillations (Lawrence et al., 1998) or inducing egg activation of mouse eggs
346 (Suzuki et al., 2010b). Our data demonstrating that $\sim 2.5 \mu\text{M}$ is the threshold concentration
347 of TPEN in eggs that first causes noticeable changes in basal Zn^{2+} , as revealed by FluoZin,

348 is consistent with the ~2 to 5 μM Zn^{2+} concentrations in most culture media without
349 serum supplementation (Lo et al., 2020), and with the ~100 pM basal Zn^{2+} in cells (Qin
350 et al., 2011). Lastly, the effects on Ca^{2+} release observed here with TPEN and other
351 chelators were due to the chelation of Zn^{2+} , as pretreatment with ZnSO_4 but not with equal
352 or greater concentrations of MgCl_2 or CaCl_2 rescued the inhibition of the responses, which
353 is consistent with results by others (Kim et al., 2010; Lawrence et al., 1998).

354 To identify how Zn^{2+} deficiency inhibits Ca^{2+} release in eggs, we induced Ca^{2+}
355 oscillations using various stimuli and tested the effectiveness of membrane-permeable
356 and impermeable chelators to abrogate them. Chelation of extracellular Zn^{2+} failed to
357 terminate the Ca^{2+} responses, whereas membrane-permeable chelators did, pointing to
358 intracellular labile Zn^{2+} levels as essential for Ca^{2+} release. All agonists used here were
359 susceptible to inhibition by TPEN, whether their activities depended on IP_3 production or
360 allosterically induced receptor function, although the effective TPEN concentrations
361 varied across stimuli. Some agents, such as *mPlcz* mRNA or thimerosal, required higher
362 concentrations than SrCl_2 , Ach, or cIP_3 . The reason underlying the different agonists'
363 sensitivities to TPEN will require additional research, but the persistence of IP_3
364 production or change in $\text{IP}_3\text{R1}$ structure needed to induce channel gating might explain
365 it. However, the universal abrogation of Ca^{2+} oscillations by TPEN supports the view
366 drawn from cryo-EM-derived $\text{IP}_3\text{R1}$ models that signaling molecules can allosterically
367 induce channel gating from different starting positions in the channel by mechanically
368 coupling the binding effect to the ion-conducting pore in the C-terminal end of IP_3R (Fan
369 et al., 2015). The cytosolic C-terminal domain of each $\text{IP}_3\text{R1}$ subunit is alongside the IP_3 -
370 binding domain of another subunit and, therefore, well positioned to sense IP_3 binding
371 and induce channel gating (Fan et al., 2015). Within each subunit, the LNK domain, which
372 contains a Zn^{2+} -finger motif (Fan et al., 2015), connects the opposite domains of the
373 molecule. Although there are no reports regarding the regulation of $\text{IP}_3\text{R1}$ sensitivity by
374 Zn^{2+} , such evidence exists for RyRs (Woodier et al., 2015), which also display a conserved
375 Zn^{2+} -finger motif (des Georges et al., 2016). Lastly, mutations of the two Cys or two His
376 residues of this motif, without exception, resulted in inhibition or inactivation of the $\text{IP}_3\text{R1}$
377 channel (Bhanumathy et al., 2012; Uchida et al., 2003). These results are consistent with
378 the view that the C-terminal end of IP_3Rs plays a dominant role in channel gating
379 (Bhanumathy et al., 2012; Uchida et al., 2003). We propose that TPEN inhibits Ca^{2+}
380 oscillations in mouse eggs because chelating Zn^{2+} interferes with the function of the LNK
381 domain and its Zn^{2+} -finger motif proposed role on the mechanical coupling induced by
382 agonist binding to the receptor that propagates to the pore-forming region and required to
383 gate the channel's ion-pore (Fan et al., 2022, 2015).

384 In support of this possibility, TPEN-induced Zn^{2+} deficient conditions altered the
385 Ca^{2+} -releasing kinetics in resting eggs or after fertilization. Tg increases intracellular Ca^{2+}
386 by inhibiting the SERCA pump (Thastrup et al., 1990) and preventing the reuptake into
387 the ER of the ebbing Ca^{2+} during the basal leak. Our previous studies showed that the
388 downregulation of IP₃R1 diminishes the leak, suggesting it occurs through IP₃R1 (Wakai
389 and Fissore, 2019). Consistent with this view, TPEN pre-treatment delayed the Ca^{2+}
390 response induced by Tg, implying that Zn^{2+} deficiency hinders Ca^{2+} release through IP₃R1.
391 An expected consequence would be increased Ca^{2+} content in the ER after Tg. Io that
392 mobilizes Ca^{2+} independently of IP₃Rs (Toeplitz et al., 1979) induced enhanced responses
393 in TPEN-treated eggs vs. controls, confirming the accumulation of Ca^{2+} - ER in Zn^{2+}
394 deficient conditions. We demonstrated that this accumulation is due to hindered emptying
395 of the Ca^{2+} ER evoked by agonists in Zn^{2+} -deficient environments resulting in reduced
396 cytosolic Ca^{2+} increases, as IP₃R1 is the pivotal intermediary channel between these
397 compartments. Noteworthy, the initial phase of the Tg-induced Ca^{2+} release out of the ER
398 did not appear modified by TPEN, as if it was mediated by a Zn^{2+} -insensitive Ca^{2+}
399 channel(s)/transporter, contrasting with Ach-induced emptying that was abrogated from
400 the outset. Remarkably, independently of Zn^{2+} chelators, emptying of Ca^{2+} ER was
401 modified in a genetic model of Zn^{2+} -deficient oocytes lacking two TRP channels,
402 confirming the impact of Zn^{2+} on Ca^{2+} release. It is worth noting that TPEN did not reduce
403 but increased the mass of IP₃R1, which might result in the inhibition of Zn^{2+} -dependent
404 ubiquitin ligase Ubc7 by the Zn-deficient conditions (Webster et al., 2003). We cannot
405 rule out that these conditions may undermine other conformational changes required to
406 trigger IP₃R1 degradation, thereby favoring the accumulation of IP₃R1.

407 Despite accruing Zn^{2+} during oocyte maturation, fertilization witnesses a
408 necessary Zn^{2+} release into the external milieu, known as “ Zn^{2+} sparks” (Kim et al., 2011;
409 Que et al., 2019, 2015). This release of Zn^{2+} is a conserved event in fertilization across
410 species and is associated with several biological functions, including those related to
411 fending off polyspermy (Kim et al., 2011; Que et al., 2019; Wozniak et al., 2020). The
412 concomitant decrease in Zn^{2+} facilitates the resumption of the cell cycle and exit from the
413 MII stage (Kim et al., 2011). Congruent with this observation, artificial manipulation that
414 maintains high Zn^{2+} levels prevent egg activation (Kim et al., 2011), whereas lowering
415 Zn^{2+} with chelators leads to egg activation without Ca^{2+} mobilization (Suzuki et al.,
416 2010b). As posed by others, these results suggest that meiosis completion and the early
417 stages of fertilization unfold within a narrow window of permissible Zn^{2+} (Kim et al.,
418 2011, 2010). Here, we extend this concept and show that IP₃R1 function and the Ca^{2+}
419 oscillations in mouse eggs require this optimal level of labile Zn^{2+} because the Ca^{2+}

420 responses interrupted by TPEN-induced Zn^{2+} -insufficiency are rescued by restoring Zn^{2+}
421 levels with ZnPT. Furthermore, unopposed increases in Zn^{2+} by exposure to ZnPT
422 abrogated fertilization-initiated Ca^{2+} oscillations and prevented the expected egg
423 activation events. It is unclear how excess Zn^{2+} disturbs the function of IP₃R1.
424 Nevertheless, IP₃R1s have multiple cysteines whose oxidation enhances the receptor
425 sensitivity to IP₃ (Joseph et al., 2018), and it is possible that excessive Zn^{2+} aberrantly
426 modifies them, disturbing IP₃R1 structure and function. These results reveal a close
427 association between the Zn^{2+} levels controlling meiotic transitions and the Ca^{2+} release
428 necessary for egg activation, placing the IP₃R1 at the center of the crosstalk of these two
429 divalent cations.

430 Abrupt Zn^{2+} changes have emerged as critical signals for meiotic and mitotic
431 transitions in oocytes, eggs, embryos, and somatic cells (Kim et al., 2011, 2010; Lo et al.,
432 2020). Fertilization relies on prototypical Ca^{2+} rises and oscillations, and Zn^{2+} sparks are
433 an egg activation event downstream of this Ca^{2+} release, establishing a functional
434 association between these two divalent cations that continues to grow (Kim et al., 2011).
435 Here, we show that, in addition, these cations actively crosstalk during fertilization and
436 that the fertilization-induced Ca^{2+} oscillations rely on optimized IP₃R1 function
437 underpinned by ideal Zn^{2+} levels set during oocyte maturation. Future studies should
438 explore if artificial alteration of Zn^{2+} levels can extend the fertile lifespan of eggs,
439 improve developmental competence, or for developing non-hormonal methods of
440 contraception.

441 **Materials and Methods**

442 **Key resources table**

Reagent type (species) or resource	Designation	Source or reference	Identifiers	Additional information
Genetic reagent (<i>Mus musculus</i>)	CD1	Charles River	022	
Genetic reagent (<i>Mus musculus</i>)	C57BL/6J	JAX	JAX: 000664	
Genetic reagent (<i>Mus musculus</i>)	<i>Trpm7</i> -floxed	A generous gift from Dr. Carmen P. Williams (NIEHS) (PMID: 30322909)		C57BL6/J and 129s4/SvJae mixed background
Genetic reagent (<i>Mus musculus</i>)	<i>Gdf9-cre</i>	JAX	JAX: 011062	
Genetic reagent (<i>Mus musculus</i>)	<i>Trpv3</i> ^{-/-}	A generous gift from Dr H. Xu (PMID: 20403327)		C57BL/6J and 129/SvEv mixed background
Biological sample (mouse oocyte)	<i>Mus musculus</i>	this paper		Eggs at the metaphase of the second meiosis
Biological sample (mouse sperm)	<i>Mus musculus</i>	this paper		Matured sperm from cauda epididymis
Recombinant DNA reagent	pcDNA6-mouse <i>Plcz1-venus</i> (plasmid used as a template for mRNA synthesis)	Published in previous Fissore lab paper PMID: 34313315. Mouse <i>Plcz1</i>		mouse <i>Plcz1</i> mRNA was fused with Venus and

		sequence was a generous gift from Dr. Kiyoko Fukami (PMID:18028898)		inserted in pcDNA6 vector
Recombinant DNA reagent	pcDNA6-CALR-D1ER-KDEL (plasmid used as a template for mRNA synthesis)	Published in previous Fissore lab paper PMID: 24101727. Original D1ER vector was a generous gift from Dr. Roger Y Tsien (PMID: 15585581)		FRET construct D1ER was inserted between ER-targeting sequence of calreticulin and KDEL ER retention signal in pcDNA6 vector
Recombinant DNA reagent	pcDNA6-human <i>ERp44-HA</i> (plasmid used as a template for mRNA synthesis)	This paper. Original human ERp44 sequence was a generous gift from Dr. Roberto Sitia (PMID: 11847130)		human <i>ERp44</i> mRNA fused with HA in pcDNA6/ Myc-His B vector
Antibody	Monoclonal HA (Mouse monoclonal)	Roche	11581816001	Dilution: 1:200
Antibody	Polyclonal IP ₃ R1 (Rabbit polyclonal)	(Parys et al., 1995)		Dilution: 1:1000
Antibody	Monoclonal α -tubulin (Mouse monoclonal)	Sigma-Aldrich	T-9026	Dilution: 1:1000
Antibody	Alexa Fluor 488 (goat anti mouse)	Invitrogen	Invitrogen: A32723	Dilution: 1:400
Commercial assay or kit	T7 mMESSAGE mMACHINE Kit	Invitrogen	Invitrogen: AM1344	Used for <i>in vitro</i> mRNA synthesis
Commercial assay or kit	Poly(A) Tailing Kit	Invitrogen	Invitrogen: AM1350	Used for poly (A)

				tailing of synthesized mRNA
Chemical compound, drug	Hyaluronidase from bovine testes	Sigma-Aldrich	H3506	
Chemical compound, drug	3-Isobutyl-1-methylxanthine (IBMX)	Sigma-Aldrich	I5879	
Chemical compound, drug	Polyvinylpyrrolidone (PVP) (average molecular weight: 360,000)	Sigma-Aldrich	PVP360	Used for mRNA microinjection and ICSI
Chemical compound, drug	N,N, N',N'-Tetrakis (2-pyridylmethyl) ethylenediamine (TPEN)	Sigma-Aldrich	P4413	Prepared in DMSO and kept at -20 °C until use
Chemical compound, drug	Zinc Pyrithione (ZnPT)	Sigma-Aldrich	PHR1401	Prepared in DMSO and kept at -20 °C until use
Chemical compound, drug	Strontium chloride hexahydrate (SrCl ₂)	Sigma-Aldrich	255521	Freshly dissolved in water on the day of experiment
Chemical compound, drug	Calcium chloride dihydrate (CaCl ₂)	Sigma-Aldrich	C3881	Freshly dissolved in water on the day of experiment
Chemical compound, drug	Magnesium chloride hexahydrate (MgCl ₂)	Sigma-Aldrich	M2393	Freshly dissolved in water on the day of experiment
Chemical compound,	Zinc sulfate monohydrate (ZnSO ₄)	Acros Organics	389802500	Freshly dissolved

drug				in water on the day of experiment
Chemical compound, drug	Ethylenediaminetetraacetic acid sodium dihydrate (EDTA)	LabChem	LC137501	Prepared as 0.5M aqueous solution with pH 8.0 adjusted by NaOH
Chemical compound, drug	Diethylenetriaminepentaacetic acid (DTPA)	Sigma-Aldrich	D6518	
Chemical compound, drug	Tris (2-pyridylmethyl) amine (TPA)	Santa Cruz	sc-477037	
Chemical compound, drug	Dimethyl sulphoxide (DMSO)	Sigma-Aldrich	D8418	Used as a solvent
Chemical compound, drug	Acetylcholine chloride	Sigma-Aldrich	A6625	
Chemical compound, drug	Thimerosal	Sigma-Aldrich	T5125	Freshly dissolved in water on the day of experiment and kept on ice until use
Chemical compound, drug	Ionomycin calcium salt	Tocris	1704	Working concentration: 2.5 μ M
Chemical compound, drug	Thapsigargin	Calbiochem	#586500	Working concentration: 10 μ M
Other	Pluronic F-127 (20% solution in DMSO) (Pluronic acid)	Invitrogen	P3000MP	
Other	Fura-2 AM	Invitrogen	F1221	Used at

				1.25 μ M in TL- HEPES containin g 0.02% Pluronic acid
Other	FluoZin-3 AM	Invitrogen	F24195	Used at 1.25 μ M in TL- HEPES containin g 0.02% Pluronic acid
Other	Fluo-4 AM	Invitrogen	F14201	Used at 1.25 μ M in TL- HEPES containin g 0.02% Pluronic acid
Other	Rhod2-AM	Invitrogen	R1244	Used at 2.2 μ M in TL- HEPES containin g 0.02% Pluronic acid.
Other	ci-IP3/ PM	Tocris	6210	Dissolved in DMSO and kept at -20° C. Before use, the stock was diluted with water to make a final concentra tion of 0.25 mM.
Other	Pme1	New England	R0560S	Used to

		BioLabs	linearize pcDNA6 vectors for mRNA synthesis
Software, algorithm	Prism	GraphPad Software	Version 5.01

443

444 N,N,N',N'-tetrakis (2-pyridinylmethyl)-1,2-ethylenediamine (TPEN) and Zinc pyrithione
445 (ZnPT) were dissolved in dimethyl sulfoxide (DMSO) at 10 mM and stored at -20°C until
446 use. SrCl₂, CaCl₂, ZnSO₄, and MgCl₂ were freshly dissolved with double-sterile water at
447 1M and diluted with the monitoring media just before use. Ethylenediaminetetraacetic
448 acid (EDTA) and diethylenetriaminepentaacetic acid (DTPA) were reconstituted with
449 double-sterile water at 0.5M and 10 mM, respectively, and the pH was adjusted to 8.0.
450 Tris(2-pyridylmethyl) amine (TPA) was diluted in DMSO at 100 mM and stored at -20°C
451 until use. Acetylcholine chloride and Thimerosal were dissolved in double-sterile water
452 at 550 mM and 100 mM, respectively. Acetylcholine was stored at -20°C until use,
453 whereas Thimerosal was made fresh in each experiment.

454

455 **Mice**

456 The University of Massachusetts Institutional Animal Care and Use Committee (IACUC)
457 approved all animal experiments and protocols. *Trpm7*-floxed (*Trpm7^{fl/fl}*) *Gdf9-Cre* and
458 *Trpv3^{-/-}* mice were bred at our facility. *Trpm7^{fl/fl}* mice were crossed with *Trpv3^{-/-}* to
459 generate *Trpm7^{fl/fl}*; *Trpv3^{-/-}* mouse line. Female *Trpm7^{fl/fl}*; *Trpv3^{-/-}* mice were crossed
460 with *Trpm7^{fl/fl}*; *Trpv3^{-/-}*; *Gdf9-cre* male to generate females null for *Trpv3* and with
461 oocyte-specific deletion for *Trpm7*. Ear clips from offspring were collected prior to
462 weaning, and confirmation of genotype was performed after most experiments.

463

464 **Egg Collection**

465 All gamete handling procedures are as previously reported by us (Wakai and Fissore,
466 2019). MII eggs were collected from the ampulla of 6- to 8-week-old female mice.
467 Females were superovulated via intraperitoneal injections of 5 IU pregnant mare serum
468 gonadotropin (PMSG, Sigma, St. Louis, MO) and 5 IU human chorionic gonadotropin
469 (hCG, sigma) at 48hr. interval. Cumulus-oocyte-complexes (COCs) were obtained 13.5
470 hr. post-hCG injection by tearing the ampulla using forceps and needles in TL-HEPES
471 medium. COCs were treated with 0.26% (w/v) of hyaluronidase at room temperature (RT)
472 for 5 min to remove cumulus cells.

473

474 **Intracytoplasmic sperm injection (ICSI)**

475 ICSI was performed as previously reported by us (Kurokawa and Fissore, 2003) using
476 described setup and micromanipulators (Narishige, Japan). Sperm from C57BL/6 or CD1
477 male mice (7-12 weeks old) were collected from the cauda epididymis in TL-HEPES
478 medium, washed several times, heads separated from tails by sonication (XL2020; Heat
479 Systems Inc., USA) for 5 s at 4°C. The sperm lysate was washed in TL-HEPES and
480 diluted with 12% polyvinylpyrrolidone (PVP, MW = 360 kDa) to a final PVP
481 concentration of 6%. A piezo micropipette-driving unit was used to deliver the sperm into
482 the ooplasm (Primetech, Ibaraki, Japan); a few piezo-pulses were applied to puncture the
483 eggs' plasma membrane following penetration of the zona pellucida. After ICSI, eggs
484 were either used for Ca²⁺ monitoring or cultured in KSOM to evaluate activation and
485 development at 36.5°C in a humidified atmosphere containing 5% CO₂.

486

487 **Preparation and microinjection of mRNA**

488 pcDNA6-*mPlcζ-mEGFP*, pcDNA6-CALR-D1ER-KDEL, and pcDNA6-*humanERp44-*
489 *HA* were linearized with the restriction enzyme PmeI and *in vitro* transcribed using the
490 T7 mMMESSAGE mMACHINE Kit following procedures previously used in our
491 laboratory (Ardestani et al., 2020). A poly(A) tail was added to the *in vitro* synthesized
492 RNA (mRNA) using Tailing Kit followed by quantification and dilution to 0.5 µg/µL in
493 nuclease-free water and stored at -80°C until use. Before microinjection, *mPlcζ*, D1ER,
494 and *ERp44* mRNA were diluted to 0.01, 1.0, and 0.5 µg/µL, respectively, in nuclease-free
495 water, heated at 95°C for 3 min followed by centrifugation at 13400×g for 10 min at 4°C.
496 Cytoplasm injection of mRNA was performed under microscopy equipped with
497 micromanipulators (Narishige, Japan). The zona pellucida and the plasma membrane of
498 MII eggs were penetrated by applying small pulses generated by the piezo
499 micromanipulator (Primetech, Ibaraki, Japan). The preparation of the injection pipette
500 was as for ICSI (Kurokawa and Fissore, 2003), but the diameter of the tip was ~1 µm.

501

502 **Ca²⁺ imaging**

503 Before Ca²⁺ imaging, eggs were incubated in TL-HEPES containing 1.25 µM Fura2-AM,
504 1.25 µM FluoZin3-AM, or 2.2 µM Rhod2-AM and 0.02% Pluronic acid for 20 min at
505 room temperature and then washed. The fluorescent probe-loaded eggs were allowed to
506 attach to the bottom of the glass dish (Mat-Tek Corp., Ashland, MA). Eggs were
507 monitored simultaneously using an inverted microscope (Nikon, Melville, NY) outfitted
508 for fluorescence measurements. Fura-2 AM, FluoZin3-AM, and Rhod2-AM fluorescence

509 were excited with 340 nm and 380 nm, 480 nm, and 550 nm wavelengths, respectively,
510 every 20 sec, for different intervals according to the experimental design and as
511 previously performed in the laboratory. The illumination was provided by a 75-W Xenon
512 arc lamp and controlled by a filter wheel (Ludl Electronic Products Ltd., Hawthorne, NY).
513 The emitted light above 510 nm was collected by a cooled Photometrics SenSys CCD
514 camera (Roper Scientific, Tucson, AZ). Nikon Element software coordinated the filter
515 wheel and data acquisition. The acquired data were saved and analyzed using Microsoft
516 Excel and GraphPad using Prism software (Ardestani et al., 2020). For Figures 1A, 4A-
517 C, 5A, and 6H-I, values obtained from FluoZin3-AM, Fura2-AM, or Rhod2-AM
518 recordings were divided by the average of the first five recordings for each treatment that
519 was used as the F_0 .

520 To estimate relative changes in Ca^{2+} -ER, emission ratio imaging of the D1ER (YFP/CFP)
521 was performed using a CFP excitation filter, dichroic beamsplitter, CFP and YFP emission
522 filters (Chroma technology, Rockingham, VT; ET436/20X, 89007bs, ET480/40m, and
523 ET535/30m). To measure Ca^{2+} -ER and cytosolic Ca^{2+} simultaneously, eggs that had been
524 injected with D1ER were loaded with Rhod-2AM, and CFP, YFP, and Rhod-2 intensities
525 were collected every 20 seconds.

526

527 **Caged IP₃**

528 Caged-IP₃/PM (cIP₃) was reconstituted in DMSO and stored at -20°C until use. Before
529 injection, cIP₃ stock was diluted to 0.25 mM with water and microinjected as above. After
530 incubation in KSOM media at 37°C for 1-hr., the injected eggs were loaded with the
531 fluorophore, 1.25 μM Fluo4-AM, and 0.02% Pluronic acid and handled as above for Fura-
532 2 AM. The release of cIP₃ was accomplished by photolysis using 0.5 to 5-sec pulses at
533 360 nm wavelengths. Ca^{2+} imaging was as above, but Fluo4 was excited at 488 nm
534 wavelength and emitted light above 510 nm collected as above.

535

536 **Western blot analysis**

537 Cell lysates from 20-50 mouse eggs were prepared by adding 2X- Laemmli sample buffer.
538 Proteins were separated on 5% SDS-PAGE gels and transferred to PVDF membranes
539 (Millipore, Bedford, MA). After blocking with 5% fat-free milk + TBS, membranes were
540 probed with the rabbit polyclonal antibody specific to IP₃R1 (1:1000; a generous gift from
541 Dr. Jan Parys, Katholieke Universiteit, Leuven, Belgium; Parys et al., 1995). Goat anti-
542 rabbit antibody conjugated to horseradish peroxidase (HRP) was used as a secondary
543 antibody (1:5000; Goat anti-Rabbit IgG (H+L) Cross-Adsorbed Secondary Antibody,
544 HRP; Invitrogen, Waltham, Ma). For detection of chemiluminescence, membranes were

545 developed using ECL Prime (Sigma) and exposed for 1–3 min to maximum sensitivity
546 film (VWR, Radnor, PA). Broad-range pre-stained SDS–PAGE molecular weight
547 markers (Bio-Rad, Hercules, CA) were run in parallel to estimate the molecular weight
548 of the immunoreactive bands. The same membranes were stripped at 50°C for 30 min
549 (62.5 mM Tris, 2% SDS, and 100 mM 2-beta mercaptoethanol) and re-probed with anti-
550 α -tubulin monoclonal antibody (1:1000).

551

552 **Immunostaining and confocal microscopy**

553 Immunostaining was performed according to our previous study (Akizawa et al., 2021).
554 After incubation with or without TPEN, MII eggs were fixed with 4% (w/v)
555 paraformaldehyde in house-made phosphate-buffered saline (PBS) for 20 min at room
556 temperature and then permeabilized for 60 min with 0.2% (v/v) Triton X-100 in PBS.
557 Next, the eggs were blocked for 45 min with a blocking buffer containing 0.2% (w/v)
558 skim milk, 2% (v/v) fetal bovine serum, 1% (w/v) bovine serum albumin, 0.1% (v/v)
559 TritonX-100, 0.75% (w/v) glycine in PBS. Eggs were incubated overnight at 4°C with
560 mouse anti-HA antibody (1:200) diluted in blocking buffer. Eggs were washed in blocking
561 buffer 3X for 10 min, followed by incubation at room temperature for 30 min with a
562 secondary antibody, Alexa Fluor 488 goat anti-mouse IgG (H + L) (1:400) diluted in
563 blocking buffer. Fluorescence signals were visualized using a laser-scanning confocal
564 microscope (Nikon A1 Resonant Confocal with six-color TIRF) fitted with a 63 \times , 1.4 NA
565 oil-immersion objective lens.

566

567 **Statistical analysis**

568 Comparisons for statistical significance of experimental values between treatments and
569 experiments were performed in three or more experiments performed on different batches
570 of eggs in most studies. Given the number of eggs needed, WB studies were repeated
571 twice. Prism-GraphPad software was used to perform the statistical comparisons that
572 include unpaired Student's t-tests, Fisher's exact test, and One-way ANOVA followed by
573 Tukey's multiple comparisons, as applicable, and the production of graphs to display the
574 data. All data are presented as mean \pm s.d. Differences were considered significant at $P <$
575 0.05.

576

577 **Acknowledgments**

578 We thank Ms. Changli He for technical support and Dr. James Chambers for support with
579 confocal microscopy support. We thank all members of the Fissore lab for useful
580 discussions and suggestions. We thank Jan B. Parys, K.U. Leuven, Belgium, for initial

581 discussions and advice.

582

583 **Competing interests**

584 The authors declare no competing or financial interests.

585

586 **Additional information**

587 **Funding Sources**

Funder	Grant reference number	Author
National Institute of Health	RO1 HD092499	Rafael A. Fissore
National Institute of Food and Agriculture	2021-06893	MG. Gervasi, R.A. Fissore, P.E. Visconti
Japan Society for the Promotion of Science Overseas Research Fellowship	Postdoctoral fellowship	Hiroki Akizawa

The funders had no role in study design, data collection and interpretation, or the decision to submit the work for publication.

588

589 **Author contributions**

590 Hiroki Akizawa, Data curation, Formal analysis, Validation, Investigation, Visualization,
591 Writing—original draft, Writing—review and editing; Emily Lopes, Data curation,
592 Formal analysis, Validation; Rafael A Fissore, Conceptualization, Formal analysis,
593 Supervision, Funding acquisition, Methodology, Writing—original draft, Project
594 administration, Writing—review and editing

595

596 **References**

597 Abbott AL, Xu Z, Kopf GS, Ducibella T, Schultz RM. 1998. In vitro culture retards
598 spontaneous activation of cell cycle progression and cortical granule exocytosis that
599 normally occur in vivo unfertilized mouse eggs. *Biol Reprod* **59**:1515–1521.
600 doi:10.1095/biolreprod59.6.1515

601 Ajduk A, Małagocki A, Maleszewski M. 2008. Cytoplasmic maturation of mammalian
602 oocytes: Development of a mechanism responsible for sperm-induced Ca²⁺
603 oscillations. *Reprod Biol* **8**:3–22. doi:10.1016/S1642-431X(12)60001-1

604 Akizawa H, Saito S, Kohri N, Furukawa E, Hayashi Y, Bai H, Nagano M, Yanagawa Y,
605 Tsukahara H, Takahashi M, Kagawa S, Kawahara-Miki R, Kobayashi H, Kono T,
606 Kawahara M. 2021. Deciphering two rounds of cell lineage segregations during
607 bovine preimplantation development. *FASEB J* **35**:1–14.
608 doi:10.1096/fj.202002762RR

- 609 Ardestani G, Mehregan A, Fleig A, Horgen FD, Carvacho I, Fissore RA. 2020. Divalent
610 cation influx and calcium homeostasis in germinal vesicle mouse oocytes. *Cell*
611 *Calcium* **87**:102181. doi:10.1016/j.ceca.2020.102181
- 612 Arslan P, Di Virgilio F, Beltrame M. 1985. Cytosolic Ca²⁺ homeostasis in Ehrlich and
613 Yoshida carcinomas. A new, membrane-permeant chelator of heavy metals reveals
614 that these ascites tumor cell lines have normal cytosolic free Ca²⁺. *J Biol Chem*
615 **260**:2719–2727. doi:10.1016/s0021-9258(18)89421-2
- 616 Barnett B, Kretshmar H, Hartman F. 1977. Structural Characterization of Bis (*j*V-
617 oxopyridine-2-thionato) zinc (II). *Inorg Chem* **16**:1834–1838.
- 618 Bernhardt ML, Kim AM, O'Halloran T V., Woodruff TK. 2011. Zinc requirement during
619 meiosis I-meiosis II transition in mouse oocytes is independent of the MOS-MAPK
620 pathway. *Biol Reprod* **84**:526–536. doi:10.1095/biolreprod.110.086488
- 621 Bernhardt ML, Kong BY, Kim AM, O'Halloran T V., Woodruff TK. 2012. A Zinc-
622 Dependent Mechanism Regulates Meiotic Progression in Mammalian Oocytes. *Biol*
623 *Reprod* **86**:1–10. doi:10.1095/biolreprod.111.097253
- 624 Bernhardt ML, Padilla-Banks E, Stein P, Zhang Y, Williams CJ. 2017. Store-operated
625 Ca²⁺ entry is not required for fertilization-induced Ca²⁺ signaling in mouse eggs.
626 *Cell Calcium* **65**:63–72. doi:10.1016/j.ceca.2017.02.004
- 627 Berridge MJ. 2016. The inositol trisphosphate/calcium signaling pathway in health and
628 disease. *Physiol Rev* **96**:1261–1296. doi:10.1152/physrev.00006.2016
- 629 Bhanumathy C, Da Fonseca PCA, Morris EP, Joseph SK. 2012. Identification of
630 functionally critical residues in the channel domain of inositol trisphosphate
631 receptors. *J Biol Chem* **287**:43674–43684. doi:10.1074/jbc.M112.415786
- 632 Bootman MD, Taylor CW, Berridge MJ. 1992. The thiol reagent, thimerosal, evokes Ca²⁺
633 spikes in HeLa cells by sensitizing the inositol 1,4,5-trisphosphate receptor. *J Biol*
634 *Chem* **267**:25113–25119. doi:10.1016/s0021-9258(19)74013-7
- 635 Brind S, Swann K, Carroll J. 2000. Inositol 1,4,5-trisphosphate receptors are
636 downregulated in mouse oocytes in response to sperm or adenophostin A but not to
637 increases in intracellular Ca²⁺ or egg activation. *Dev Biol* **223**:251–265.
638 doi:10.1006/dbio.2000.9728
- 639 Broun ER, Greist A, Tricot G, Hoffman R. 1990. Excessive Zinc Ingestion: A Reversible
640 Cause of Sideroblastic Anemia and Bone Marrow Depression. *JAMA J Am Med*
641 *Assoc* **264**:1441–1443. doi:10.1001/jama.1990.03450110087033
- 642 Carraway RE, Dobner PR. 2012. Zinc pyrithione induces ERK- and PKC-dependent
643 necrosis distinct from TPEN-induced apoptosis in prostate cancer cells. *Biochim*
644 *Biophys Acta - Mol Cell Res* **1823**:544–557. doi:10.1016/j.bbamcr.2011.09.013

- 645 Carvacho I, Ardestani G, Lee HC, McGarvey K, Fissore RA, Lykke-Hartmann K. 2016.
646 TRPM7-like channels are functionally expressed in oocytes and modulate post-
647 fertilization embryo development in mouse. *Sci Rep* **6**:1–12. doi:10.1038/srep34236
- 648 Carvacho I, Lee HC, Fissore RA, Clapham DE. 2013. TRPV3 Channels mediate
649 strontium-induced mouse-egg activation. *Cell Rep* **5**:1375–1386.
650 doi:10.1016/j.celrep.2013.11.007
- 651 Deguchi R, Shirakawa H, Oda S, Mohri T, Miyazaki S. 2000. Spatiotemporal analysis of
652 Ca²⁺ waves in relation to the sperm entry site and animal-vegetal axis during Ca²⁺
653 oscillations in fertilized mouse eggs. *Dev Biol* **218**:299–313.
654 doi:10.1006/dbio.1999.9573
- 655 des Georges A, Clarke OB, Zalk R, Yuan Q, Condon KJ, Grassucci RA, Hendrickson WA,
656 Marks AR, Frank J. 2016. Structural Basis for Gating and Activation of RyR1. *Cell*
657 **167**:145–157.e17. doi:10.1016/j.cell.2016.08.075
- 658 Ducibella T, Huneau D, Angelichio E, Xu Z, Schultz RM, Kopf GS, Fissore R, Madoux
659 S, Ozil J-P. 2002. Egg-to-Embryo Transition Is Driven by Differential Responses to
660 Ca²⁺ Oscillation Number. *Dev Biol* **250**:280–291. doi:10.1006/dbio.2002.0788
- 661 Dupont G, McGuinness OM, Johnson MH, Berridge MJ, Borgese F. 1996. Phospholipase
662 C in mouse oocytes: Characterization of β and γ isoforms and their possible
663 involvement in sperm-induced Ca²⁺ spiking. *Biochem J* **316**:583–591.
664 doi:10.1042/bj3160583
- 665 Eppig JJ. 1996. Coordination of nuclear and cytoplasmic oocyte maturation in eutherian
666 mammals. *Reprod Fertil Dev* **8**:485–489. doi:10.1071/RD9960485
- 667 Evellin S, Nolte J, Tysack K, Dorp F Vom, Thiel M, Oude Weernink PA, Jakobs KH,
668 Webb EJ, Lomasney JW, Schmidt M. 2002. Stimulation of phospholipase C- ϵ by the
669 M3 muscarinic acetylcholine receptor mediated by cyclic AMP and the GTPase
670 Rap2B. *J Biol Chem* **277**:16805–16813. doi:10.1074/jbc.M112024200
- 671 Fan G, Baker ML, Wang Z, Baker MR, Sinyagovskiy PA, Chiu W, Ludtke SJ, Serysheva
672 II. 2015. Gating machinery of InsP3R channels revealed by electron cryomicroscopy.
673 *Nature* **527**:336–341. doi:10.1038/nature15249
- 674 Fan G, Baker MR, Terry LE, Arige V, Chen M, Seryshev AB, Baker ML, Ludtke SJ, Yule
675 DI, Serysheva II. 2022. Conformational motions and ligand-binding underlying
676 gating and regulation in IP3R channel. *Nat Commun* **13**:1–15. doi:10.1038/s41467-
677 022-34574-1
- 678 Fissore RA, Longo FJ, Anderson E, Parys JB, Ducibella T. 1999. Differential distribution
679 of inositol trisphosphate receptor isoforms in mouse oocytes. *Biol Reprod* **60**:49–57.
680 doi:10.1095/biolreprod60.1.49

- 681 Fujiwara T, Nakada K, Shirakawa H, Shunichi M. 1993. Development of inositol
682 trisphosphate-induced calcium release mechanism during maturation of hamster
683 oocytes. *Dev Biol*.
- 684 Hajnóczky G, Thomas AP. 1997. Minimal requirements for calcium oscillations driven
685 by the IP3 receptor. *EMBO J* **16**:3533–3543. doi:10.1093/emboj/16.12.3533
- 686 Hamada K, Terauchi A, Mikoshiba K. 2003. Three-dimensional Rearrangements within
687 Inositol 1,4,5-Trisphosphate Receptor by Calcium. *J Biol Chem* **278**:52881–52889.
688 doi:10.1074/jbc.M309743200
- 689 Hara T, Yoshigai E, Ohashi T, Fukada T. 2022. Zinc transporters as potential therapeutic
690 targets: An updated review. *J Pharmacol Sci* **148**:221–228.
691 doi:10.1016/j.jphs.2021.11.007
- 692 Heim A, Tischer T, Mayer TU. 2018. Calcineurin promotes APC/C activation at meiotic
693 exit by acting on both XErp1 and Cdc20. *EMBO Rep* **19**:1–10.
694 doi:10.15252/embr.201846433
- 695 Higo T, Hattori M, Nakamura T, Natsume T, Michikawa T, Mikoshiba K. 2005. Subtype-
696 specific and ER lumenal environment-dependent regulation of inositol 1,4,5-
697 trisphosphate receptor type 1 by ERp44. *Cell* **120**:85–98.
698 doi:10.1016/j.cell.2004.11.048
- 699 Iino M. 1990. Biphasic Ca²⁺ dependence of inositol 1,4,5-trisphosphate-induced Ca
700 release in smooth muscle cells of the guinea pig taenia caeci. *J Gen Physiol* **95**:1103–
701 1122. doi:10.1085/jgp.95.6.1103
- 702 Jean T, Klee CB. 1986. Calcium modulation of inositol 1,4,5-trisphosphate-induced
703 calcium release from neuroblastoma x glioma hybrid (NG108-15) microsomes. *J*
704 *Biol Chem* **261**:16414–16420. doi:10.1016/s0021-9258(18)66582-2
- 705 Jellerette T, He CL, Wu H, Parys JB, Fissore RA. 2000. Down-regulation of the Inositol
706 1,4,5-Triphosphate Receptor in Mouse Eggs Following Fertilization or
707 Parthenogenetic Activation. *Dev Biol* **223**:238–250. doi:10.1006/dbio.2000.9675
- 708 Jellerette T, Kurokawa M, Lee B, Malcuit C, Yoon SY, Smyth J, Vermassen E, De Smedt
709 H, Parys JB, Fissore RA. 2004. Cell cycle-coupled [Ca²⁺]_i oscillations in mouse
710 zygotes and function of the inositol 1,4,5-trisphosphate receptor-1. *Dev Biol* **274**:94–
711 109. doi:10.1016/j.ydbio.2004.06.020
- 712 Joseph SK, Young MP, Alzayady K, Yule DI, Ali M, Booth DM, Hajnóczky G. 2018.
713 Redox regulation of type-I inositol trisphosphate receptors in intact mammalian cells.
714 *J Biol Chem* **293**:17464–17476. doi:10.1074/jbc.RA118.005624
- 715 Kang D, Park JY, Han J, Bae IH, Yoon SY, Kang SS, Choi WS, Hong SG. 2003.
716 Acetylcholine induces Ca²⁺ oscillations via m3/m4 muscarinic receptors in the

- 717 mouse oocyte. *Pflugers Arch Eur J Physiol* **447**:321–327. doi:10.1007/s00424-003-
718 1184-y
- 719 Kaur K, Gupta R, Saraf SA, Saraf SK. 2014. Zinc: The metal of life. *Compr Rev Food*
720 *Sci Food Saf* **13**:358–376. doi:10.1111/1541-4337.12067
- 721 Kim AM, Bernhardt ML, Kong BY, Ahn RW, Vogt S, Woodruff TK, O’Halloran T V. 2011.
722 Zinc sparks are triggered by fertilization and facilitate cell cycle resumption in
723 mammalian eggs. *ACS Chem Biol* **6**:716–723. doi:10.1021/cb200084y
- 724 Kim AM, Vogt S, O’Halloran T V., Woodruff TK. 2010. Zinc availability regulates exit
725 from meiosis in maturing mammalian oocytes. *Nat Chem Biol* **6**:674–681.
726 doi:10.1038/nchembio.419
- 727 Kurokawa M, Fissore RA. 2003. ICSI-generated mouse zygotes exhibit altered calcium
728 oscillations, inositol 1,4,5-trisphosphate receptor-1 down-regulation, and embryo
729 development. *Mol Hum Reprod* **9**:523–533. doi:10.1093/molehr/gag072
- 730 Lawrence Y, Ozil JP, Swann K. 1998. The effects of a Ca²⁺ chelator and heavy-metal-ion
731 chelators upon Ca²⁺ oscillations and activation at fertilization in mouse eggs suggest
732 a role for repetitive Ca²⁺ increases. *Biochem J* **335**:335–342.
733 doi:10.1042/bj3350335
- 734 Lee B, Vermassen E, Yoon SY, Vanderheyden V, Ito J, Alfandari D, De Smedt H, Parys
735 JB, Fissore RA. 2006. Phosphorylation of IP3R1 and the regulation of [Ca²⁺]_i
736 responses at fertilization: A role for the MAP kinase pathway. *Development*
737 **133**:4355–4365. doi:10.1242/dev.02624
- 738 Lemos FO, Bultynck G, Parys JB. 2021. A comprehensive overview of the complex world
739 of the endo- and sarcoplasmic reticulum Ca²⁺-leak channels. *Biochim Biophys Acta*
740 *- Mol Cell Res* **1868**:119020. doi:10.1016/j.bbamcr.2021.119020
- 741 Liu M. 2011. The biology and dynamics of mammalian cortical granules. *Reprod Biol*
742 *Endocrinol* **9**:1–17. doi:10.1186/1477-7827-9-149
- 743 Lo MN, Damon LJ, Tay JW, Jia S, Palmer AE. 2020. Single cell analysis reveals multiple
744 requirements for zinc in the mammalian cell cycle. *Elife* **9**:1–24.
745 doi:10.7554/eLife.51107
- 746 Lorca T, Cruzalegui FH, Fesquet D, Cavadore J, Méry J, Means A, Marcel D. 1993.
747 Calmodulin-dependent protein kinase II mediates inactivation of MPF and CSF upon
748 fertilization of *Xenopus* eggs. *Nature* **366**:270–273.
- 749 Maret W, Li Y. 2009. Coordination dynamics of zinc in proteins. *Chem Rev* **109**:4682–
750 4707. doi:10.1021/cr800556u
- 751 Matsu-ura T, Shirakawa H, Suzuki KGN, Miyamoto A, Sugiura K, Michikawa T, Kusumi
752 A, Mikoshiba K. 2019. Dual-FRET imaging of IP 3 and Ca 2+ revealed Ca 2+ -

- 753 induced IP₃ production maintains long lasting Ca²⁺ oscillations in fertilized mouse
754 eggs. *Sci Rep* **9**:1–11. doi:10.1038/s41598-019-40931-w
- 755 Mendivil-Perez M, Velez-Pardo C, Jimenez-Del-Rio M. 2012. TPEN induces apoptosis
756 independently of zinc chelator activity in a model of acute lymphoblastic leukemia
757 and Ex vivo acute leukemia cells through oxidative stress and mitochondria caspase-
758 3- and AIF-dependent pathways. *Oxid Med Cell Longev* **2012**.
759 doi:10.1155/2012/313275
- 760 Miao YL, Stein P, Jefferson WN, Padilla-Banks E, Williams CJ. 2012. Calcium influx-
761 mediated signaling is required for complete mouse egg activation. *Proc Natl Acad*
762 *Sci U S A* **109**:4169–4174. doi:10.1073/pnas.1112333109
- 763 Miyazaki S. 1988. Inositol 1,4,5-trisphosphate-induced calcium release and guanine
764 nucleotide-binding protein-mediated periodic calcium rises in golden hamster eggs.
765 *J Cell Biol* **106**:345–353.
- 766 Miyazaki S, Ito M. 2006. Calcium signals for egg activation in mammals. *J Pharmacol*
767 *Sci* **100**:545–552. doi:10.1254/jphs.CPJ06003X
- 768 Miyazaki SI, Hashimoto N, Yoshimoto Y, Kishimoto T, Igusa Y, Hiramoto Y. 1986.
769 Temporal and spatial dynamics of the periodic increase in intracellular free calcium
770 at fertilization of golden hamster eggs. *Dev Biol* **118**:259–267. doi:10.1016/0012-
771 1606(86)90093-X
- 772 Miyazaki SI, Yuzaki M, Nakada K, Shirakawa H, Nakanishi S, Nakade S, Mikoshiba K.
773 1992. Block of Ca²⁺ wave and Ca²⁺ oscillation by antibody to the inositol 1,4,5-
774 trisphosphate receptor in fertilized hamster eggs. *Science (80-)* **257**:251–255.
775 doi:10.1126/science.1321497
- 776 Nomikos M, Elgmati K, Theodoridou M, Calver BL, Nounesis G, Swann K, Lai FA. 2011.
777 Phospholipase C ζ binding to PtdIns(4,5)P₂ requires the XY-linker region. *J Cell Sci*
778 **124**:2582–2590. doi:10.1242/jcs.083485
- 779 Nomikos M, Sanders JR, Parthimos D, Buntwal L, Calver BL, Stamatiadis P, Smith A,
780 Clue M, Sideratou Z, Swann K, Lai FA. 2015. Essential role of the EF-hand domain
781 in targeting sperm phospholipase C ζ to membrane phosphatidylinositol 4,5-
782 bisphosphate (PIP₂). *J Biol Chem* **290**:29519–29530. doi:10.1074/jbc.M115.658443
- 783 Pace NJ, Weerapana E. 2014. A competitive chemical-proteomic platform to identify
784 zinc-binding cysteines. *ACS Chem Biol* **9**:258–265. doi:10.1021/cb400622
- 785 Paknejad N, Hite RK. 2018. Structural basis for the regulation of inositol trisphosphate
786 receptors by Ca²⁺ and IP₃. *Nat Struct Mol Biol* **25**:660–668. doi:10.1038/s41594-
787 018-0089-6
- 788 Palmer AE, Jin C, Reed JC, Tsien RY. 2004. Bcl-2-mediated alterations in endoplasmic

- 789 reticulum Ca²⁺ analyzed with an improved genetically encoded fluorescent sensor.
790 *Proc Natl Acad Sci U S A* **101**:17404–17409. doi:10.1073/pnas.0408030101
- 791 Parrington J, Brind S, De Smedt H, Gangeswaran R, Anthony Lai F, Wojcikiewicz R,
792 Carroll J. 1998. Expression of inositol 1,4,5-trisphosphate receptors in mouse
793 oocytes and early embryos: The type I isoform is upregulated in oocytes and
794 downregulated after fertilization. *Dev Biol* **203**:451–461.
795 doi:10.1006/dbio.1998.9071
- 796 Parys JB, De Smedt H, Missiaen L, Bootman MD, Sienaert I, Casteels R. 1995. Rat
797 basophilic leukemia cells as model system for inositol 1,4,5-trisphosphate receptor
798 IV, a receptor of the type II family: functional comparison and immunological
799 detection. *Cell Calcium* **17**:239–249. doi:10.1016/0143-4160(95)90070-5
- 800 Perreault SD, Barbee RR, Slott VL. 1988. Importance of glutathione in the acquisition
801 and maintenance of sperm nuclear decondensing activity in maturing hamster
802 oocytes. *Dev Biol* **125**:181–186. doi:10.1016/0012-1606(88)90070-X
- 803 Qin Y, Dittmer PJ, Park JG, Jansen KB, Palmer AE. 2011. Measuring steady-state and
804 dynamic endoplasmic reticulum and Golgi Zn²⁺ with genetically encoded sensors.
805 *Proc Natl Acad Sci U S A* **108**:7351–7356. doi:10.1073/pnas.1015686108
- 806 Que EL, Bleher R, Duncan FE, Kong BY, Gleber SC, Vogt S, Chen S, Garwin SA, Bayer
807 AR, Dravid VP, Woodruff TK, O'Halloran T V. 2015. Quantitative mapping of zinc
808 fluxes in the mammalian egg reveals the origin of fertilization-induced zinc sparks.
809 *Nat Chem* **7**:130–139. doi:10.1038/nchem.2133
- 810 Que EL, Duncan FE, Lee HC, Hornick JE, Vogt S, Fissore RA, O'Halloran T V., Woodruff
811 TK. 2019. Bovine eggs release zinc in response to parthenogenetic and sperm-
812 induced egg activation. *Theriogenology* **127**:41–48.
813 doi:10.1016/j.theriogenology.2018.12.031
- 814 Richardson A, Taylor CW. 1993. Effects of Ca²⁺ chelators on purified inositol 1,4,5-
815 trisphosphate (InsP₃) receptors and InsP₃-stimulated Ca²⁺ mobilization. *J Biol*
816 *Chem* **268**:11528–11533. doi:10.1016/s0021-9258(19)50232-0
- 817 Ridgway EB, Gilkey JC, Jaffe LF. 1977. Free calcium increases explosively in activating
818 medaka eggs. *Proc Natl Acad Sci U S A* **74**:623–627. doi:10.1073/pnas.74.2.623
- 819 Robinson MA. 1964. Complexes of 1-hydroxy 2-pyridinethione. *J Inorg Nucl Chem*
820 **26**:1277–1281. doi:10.1016/0022-1902(64)80210-4
- 821 Sanders JR, Ashley B, Moon A, Woolley TE, Swann K. 2018. PLC ζ induced Ca²⁺
822 oscillations in mouse eggs involve a positive feedback cycle of Ca²⁺ induced InsP₃
823 formation from cytoplasmic PIP₂. *Front Cell Dev Biol* **6**:1–14.
824 doi:10.3389/fcell.2018.00036

- 825 Saunders CM, Larman MG, Parrington J, Cox LJ, Royse J, Blayney LM, Swann K, Lai
826 FA. 2002. PLC zeta: a sperm-specific trigger of Ca²⁺ oscillations in eggs and
827 embryo development. *Development* **129**:3533–44.
- 828 Schultz RM, Kopf GS. 1995. Molecular Basis of Mammalian Egg Activation. *Curr Top*
829 *Dev Biol* **30**:21–62. doi:10.1007/978-3-642-83139-3_7
- 830 Shoji S, Muto Y, Ikeda M, He F, Tsuda K, Ohsawa N, Akasaka R, Terada T, Wakiyama
831 M, Shirouzu M, Yokoyama S. 2014. The zinc-binding region (ZBR) fragment of
832 Emi2 can inhibit APC/C by targeting its association with the coactivator Cdc20 and
833 UBE2C-mediated ubiquitylation. *FEBS Open Bio* **4**:689–703.
834 doi:10.1016/j.fob.2014.06.010
- 835 Shoji S, Yoshida N, Amanai M, Ohgishi M, Fukui T, Fujimoto S, Nakano Y, Kajikawa E,
836 Perry ACF. 2006. Mammalian Emi2 mediates cytostatic arrest and transduces the
837 signal for meiotic exit via Cdc20. *EMBO J* **25**:834–845.
838 doi:10.1038/sj.emboj.7600953
- 839 Sienaert I, Missiaen L, De Smedt H, Parys JB, Sipma H, Casteels R. 1997. Molecular and
840 functional evidence for multiple Ca²⁺-binding domains in the type 1 inositol 1,4,5-
841 trisphosphate receptor. *J Biol Chem* **272**:25899–25906.
842 doi:10.1074/jbc.272.41.25899
- 843 Sikora J, Ouagazzal AM. 2021. Synaptic zinc: An emerging player in Parkinson’s disease.
844 *Int J Mol Sci* **22**:1–16. doi:10.3390/ijms22094724
- 845 Sipma H, De Smet P, Sienaert I, Vanlingen S, Missiaen L, Parys JB, De Smedt H. 1999.
846 Modulation of inositol 1,4,5-trisphosphate binding to the recombinant ligand-
847 binding site of the type-1 inositol 1,4,5-trisphosphate receptor by Ca²⁺ and
848 calmodulin. *J Biol Chem* **274**:12157–12162. doi:10.1074/jbc.274.17.12157
- 849 Snitsarev VA, McNulty TJ, Taylor CW. 1996. Endogenous heavy metal ions perturb fura-
850 2 measurements of basal and hormone-evoked Ca²⁺ signals. *Biophys J* **71**:1048–
851 1056. doi:10.1016/S0006-3495(96)79305-0
- 852 Stein P, Savy V, Williams AM, Williams CJ. 2020. Modulators of calcium signalling at
853 fertilization. *Open Biol* **10**. doi:10.1098/rsob.200118
- 854 Stricker SA. 1999. Comparative biology of calcium signaling during fertilization and egg
855 activation in animals. *Dev Biol* **211**:157–176. doi:10.1006/dbio.1999.9340
- 856 Suzuki T, Suzuki E, Yoshida N, Kubo A, Li H, Okuda E, Amanai M, Perry ACF. 2010a.
857 Mouse Emi2 as a distinctive regulatory hub in second meiotic metaphase.
858 *Development* **137**:3281–3291. doi:10.1242/dev.052480
- 859 Suzuki T, Yoshida N, Suzuki E, Okuda E, Perry ACF. 2010b. Full-term mouse
860 development by abolishing Zn²⁺-dependent metaphase II arrest without Ca²⁺

- 861 release. *Development* **137**:2659–2669. doi:10.1242/dev.049791
- 862 Swann K, Parrington J. 1999. Mechanism of Ca²⁺ release at fertilization in mammals. *J*
863 *Exp Zool* **285**:267–275. doi:10.1002/(SICI)1097-010X(19991015)285:3<267::AID-
864 JEZ10>3.0.CO;2-P
- 865 Taylor CW, Tovey SC. 2010. IP₃ Receptors: Toward Understanding Their Activation.
866 *Cold Spring Harb Perspect Biol* **2**:1–23.
- 867 Thastrup O, Cullen PJ, Drobak BK, Hanley MR, Dawson AP. 1990. Thapsigargin, a tumor
868 promoter, discharges intracellular Ca²⁺ stores by specific inhibition of the
869 endoplasmic reticulum Ca²⁺-ATPase. *Proc Natl Acad Sci U S A* **87**:2466–2470.
870 doi:10.1073/pnas.87.7.2466
- 871 Toeplitz BK, Cohen AI, Funke PT, Parker WL, Gougoutas JZ. 1979. Structure of
872 Ionomycin—A Novel Diacidic Polyether Antibiotic Having High Affinity for
873 Calcium Ions. *J Am Chem Soc* **101**:3344–3353. doi:10.1021/ja00506a035
- 874 Tokuhiro K, Dean J. 2018. Glycan-Independent Gamete Recognition Triggers Egg Zinc
875 Sparks and ZP2 Cleavage to Prevent Polyspermy. *Dev Cell* **46**:627-640.e5.
876 doi:10.1016/j.devcel.2018.07.020
- 877 Uchida K, Miyauchi H, Furuichi T, Michikawa T, Mikoshiba K. 2003. Critical regions
878 for activation gating of the inositol 1,4,5-trisphosphate receptor. *J Biol Chem*
879 **278**:16551–16560. doi:10.1074/jbc.M300646200
- 880 Wakai T, Fissore RA. 2019. Constitutive IP₃R1-mediated Ca²⁺ release reduces Ca²⁺
881 store content and stimulates mitochondrial metabolism in mouse GV oocytes. *J Cell*
882 *Sci* **132**. doi:10.1242/jcs.225441
- 883 Wakai T, Fissore RA. 2013. Ca²⁺ homeostasis and regulation of ER Ca²⁺ in mammalian
884 oocytes/eggs. *Cell Calcium* **53**:63–67. doi:10.1016/j.ceca.2012.11.010
- 885 Wakai T, Harada Y, Miyado K, Kono T. 2014. Mitochondrial dynamics controlled by
886 mitofusins define organelle positioning and movement during mouse oocyte
887 maturation. *Mol Hum Reprod* **20**:1090–1100. doi:10.1093/molehr/gau064
- 888 Wakai T, Mehregan A, Fissore RA. 2019. Ca²⁺ signaling and homeostasis in mammalian
889 oocytes and eggs. *Cold Spring Harb Perspect Biol* **11**.
890 doi:10.1101/cshperspect.a035162
- 891 Wakai T, Vanderheyden V, Yoon SY, Cheon B, Zhang N, Parys JB, Fissore RA. 2012.
892 Regulation of inositol 1,4,5-trisphosphate receptor function during mouse oocyte
893 maturation. *J Cell Physiol* **227**:705–717. doi:10.1002/jcp.22778
- 894 Wakai T, Zhang N, Vangheluwe P, Fissore RA. 2013. Regulation of endoplasmic
895 reticulum Ca²⁺ oscillations in mammalian eggs. *J Cell Sci* **126**:5714–5724.
896 doi:10.1242/jcs.136549

- 897 Walker JW, Somlyo A V., Goldman YE, Somlyo AP, Trentham DR. 1987. Kinetics of
898 smooth and skeletal muscle activation by laser pulse photolysis of caged inositol
899 1,4,5-trisphosphate. *Nature* **327**:249–252.
- 900 Watanabe S, Amagai Y, Sannino S, Tempio T, Anelli T, Harayama M, Masui S, Sorrentino
901 I, Yamada M, Sitia R, Inaba K. 2019. Zinc regulates ERp44-dependent protein
902 quality control in the early secretory pathway. *Nat Commun* **10**:1–16.
903 doi:10.1038/s41467-019-08429-1
- 904 Webster JM, Tiwari S, Weissman AM, Wojcikiewicz RJH. 2003. Inositol 1,4,5-
905 trisphosphate receptor ubiquitination is mediated by mammalian Ubc7, a component
906 of the endoplasmic reticulum-associated degradation pathway, and is inhibited by
907 chelation of intracellular Zn²⁺. *J Biol Chem* **278**:38238–38246.
908 doi:10.1074/jbc.M305600200
- 909 Woodier J, Rainbow RD, Stewart AJ, Pitt SJ. 2015. Intracellular zinc modulates cardiac
910 ryanodine receptor-mediated calcium release. *J Biol Chem* **290**:17599–17610.
911 doi:10.1074/jbc.M115.661280
- 912 Wozniak KL, Bainbridge RE, Summerville DW, Tembo M, Phelps WA, Sauer ML,
913 Wisner BW, Czekalski ME, Pasumathy S, Hanson ML, Linderman MB, Luu CH,
914 Boehm ME, Sanders SM, Buckley KM, Bain DJ, Nicotra ML, Lee MT, Carlson AE.
915 2020. Zinc protection of fertilized eggs is an ancient feature of sexual reproduction
916 in animals. *PLoS Biol* **18**:1–17. doi:10.1371/journal.pbio.3000811
- 917 Wu H, Smyth J, Luzzi V, Fukami K, Takenawa T, Black SL, Allbritton NL, Fissore RA.
918 2001. Sperm factor induces intracellular free calcium oscillations by stimulating the
919 phosphoinositide pathway. *Biol Reprod* **64**:1338–1349.
920 doi:10.1095/biolreprod64.5.1338
- 921 Wu L, Sweet T, Clapham DE. 2010. Current Progress in the Mammalian TRP Ion Channel
922 Family. *Pharmacol Rev* **62**:381–404. doi:10.1124/pr.110.002725. Abbreviations
- 923 Xu Z, Williams CJ, Kopf GS, Schultz RM. 2003. Maturation-associated increase in IP3
924 receptor type 1: Role in conferring increased IP3 sensitivity and Ca²⁺ oscillatory
925 behavior in mouse eggs. *Dev Biol* **254**:163–171. doi:10.1016/S0012-
926 1606(02)00049-0
- 927 Yamasaki S, Sakata-Sogawa K, Hasegawa A, Suzuki T, Kabu K, Sato E, Kurosaki T,
928 Yamashita S, Tokunaga M, Nishida K, Hirano T. 2007. Zinc is a novel intracellular
929 second messenger. *J Cell Biol* **177**:637–645. doi:10.1083/jcb.200702081
- 930 Zhang N, Duncan FE, Que EL, O’Halloran T V., Woodruff TK. 2016. The fertilization-
931 induced zinc spark is a novel biomarker of mouse embryo quality and early
932 development. *Sci Rep* **6**:1–9. doi:10.1038/srep22772

934 **Table**

935 **Table 1. Addition of TPEN after ICSI does not prevent extrusion of the second polar**
936 **body but precludes pronuclear (PN) formation.**

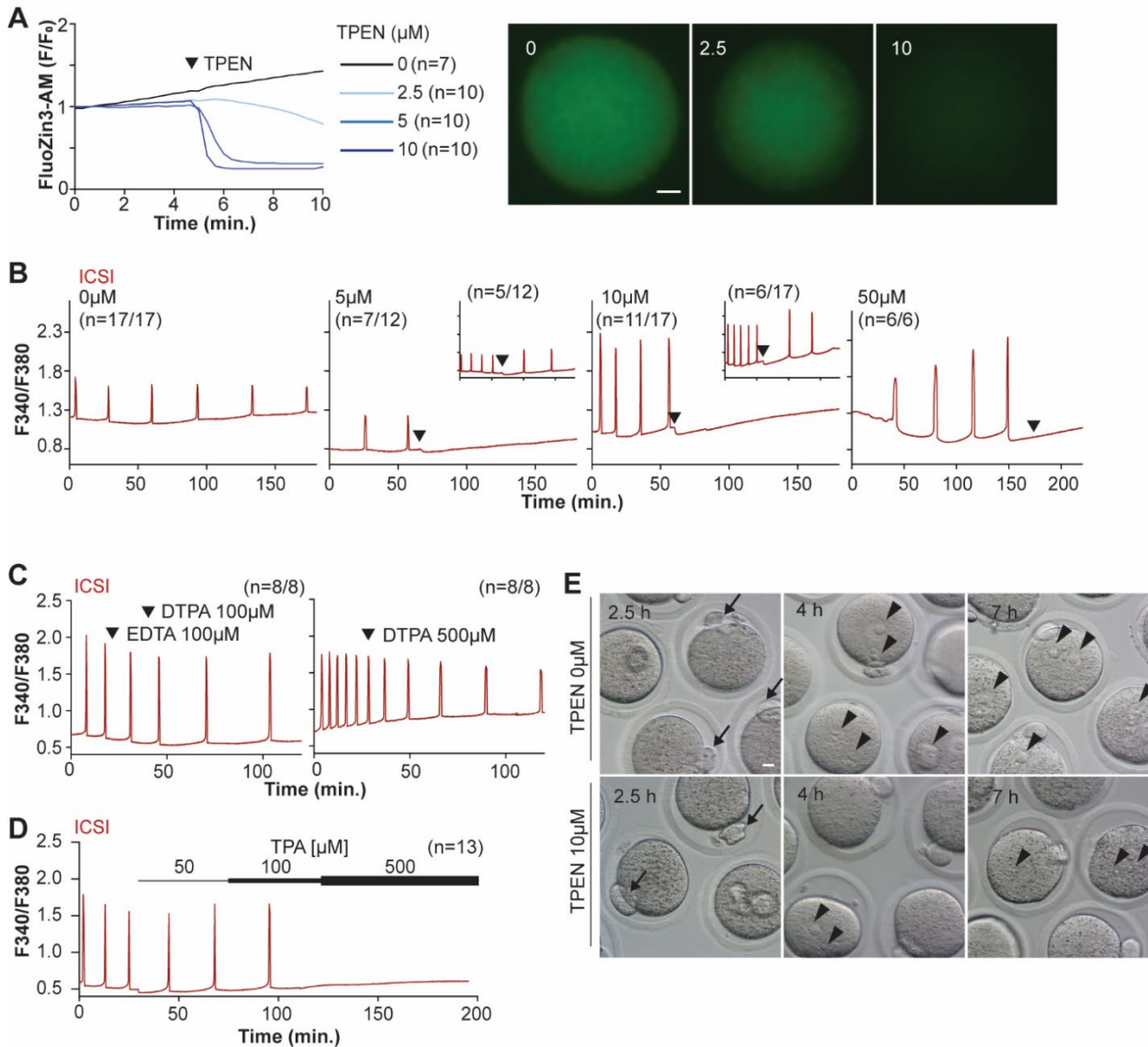
Group*	No. of zygotes	2 nd polar body (2.5h)	PN	
			4h	7h
Untreated	26	25 (96.1%)	23 (88.5%)	23 (88.5%)
TPEN (10 μ M)	27	24 (88.9%)	1 (3.7%)***	2 (7.4%)***

937 *** $P < 0.001$

938 *Data from three different replicates for each group.

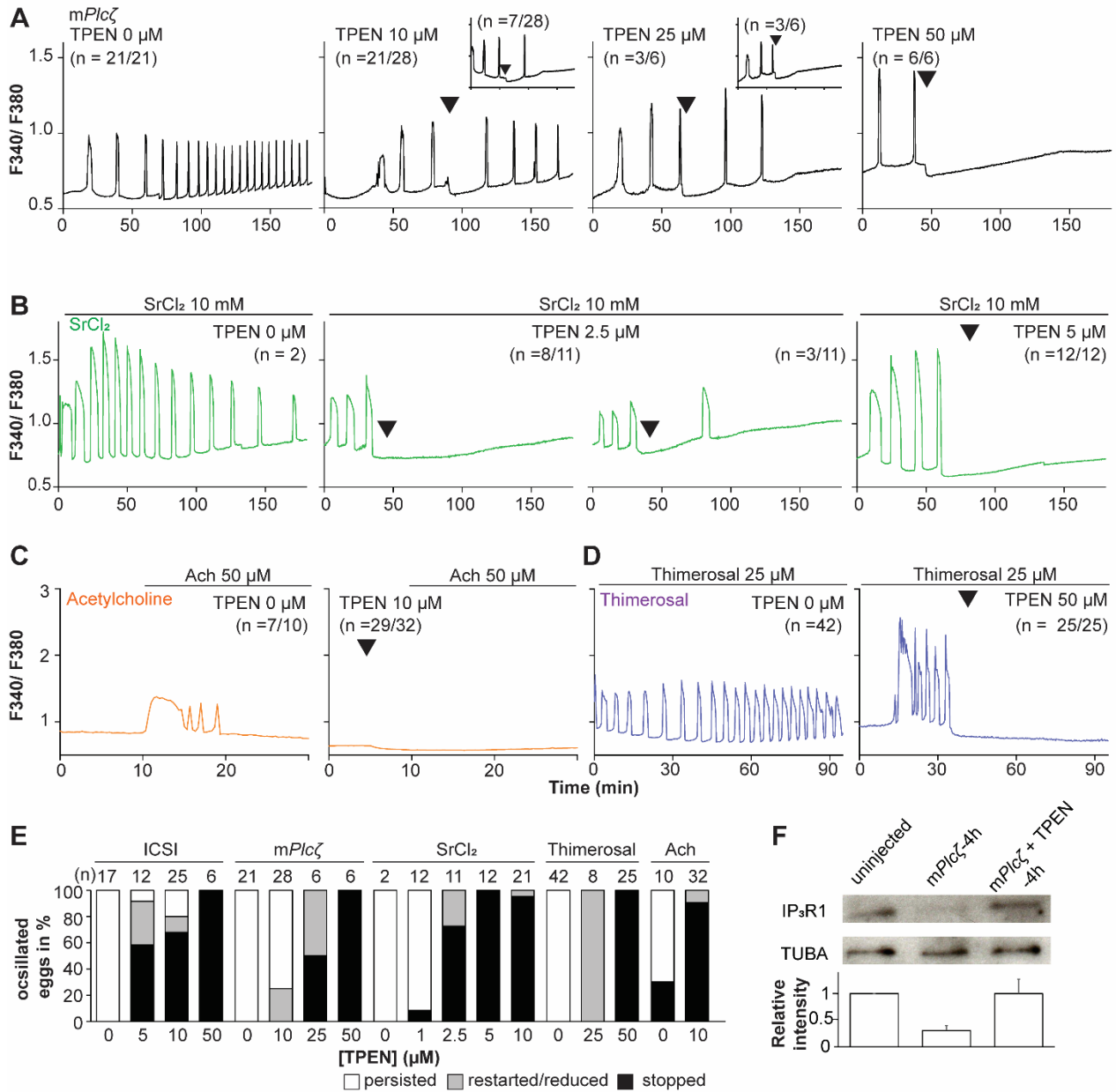
939 **Figures and Legends**

940 **Figure 1. TPEN-induced Zn²⁺ deficiency inhibits fertilization-initiated Ca²⁺ oscillations in a**
 941 **dose-dependent manner.**



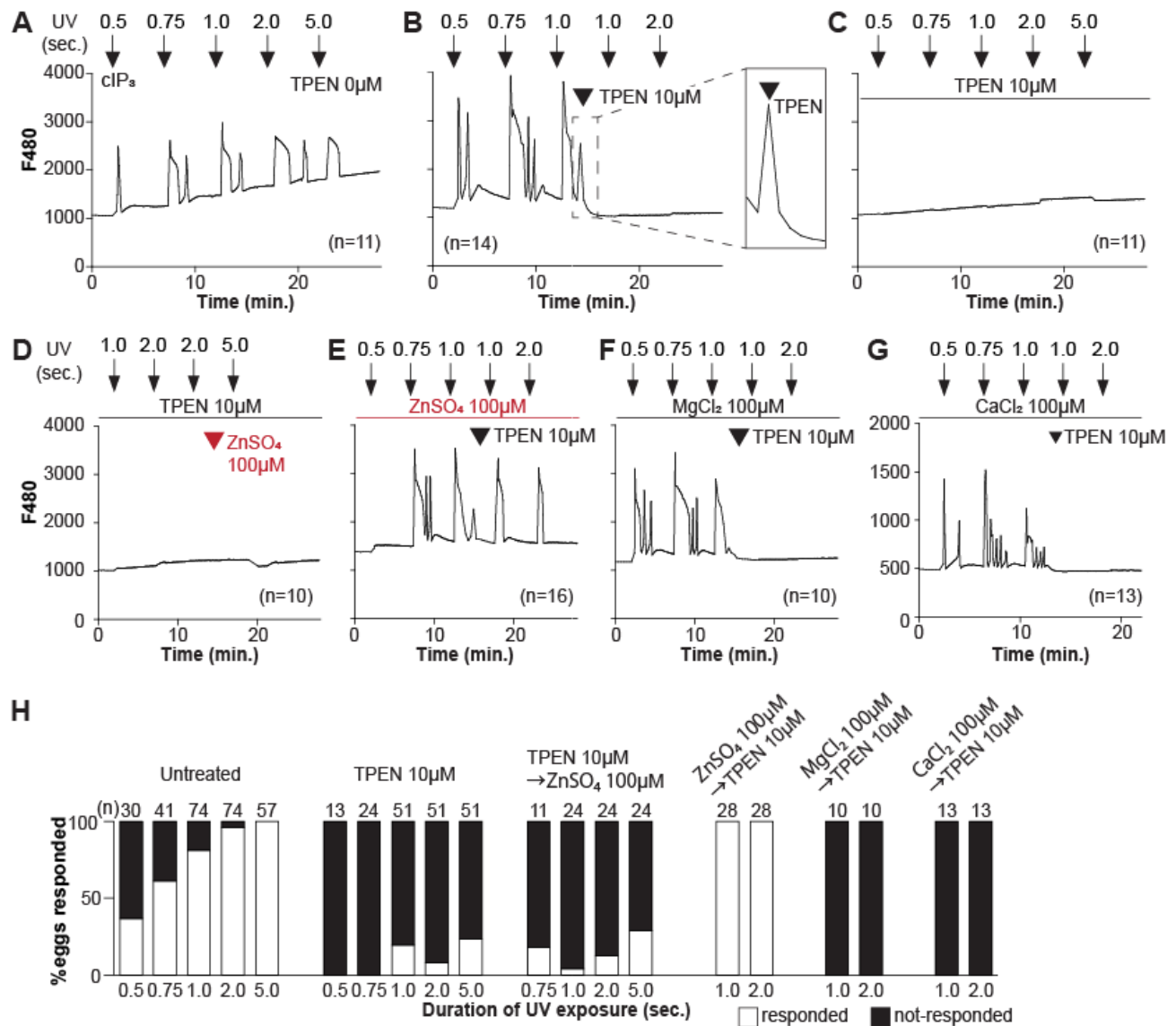
942
 943 (A) (Left panel) Representative normalized Zn²⁺ recordings of MII eggs loaded with FluoZin-3AM
 944 following the addition of increasing concentrations of TPEN (0 μM, DMSO, black trace; 2.5 μM, sky
 945 blue; 5 μM, blue; 10 μM, navy). TPEN was directly added to the monitoring media. (Right panel)
 946 Representative fluorescent images of MII eggs loaded FluoZin-3AM supplemented with 0, 2.5, and 10
 947 μM of TPEN. Scale bar: 10 μm. (B-D). (B) Representative Ca²⁺ oscillations following ICSI after the
 948 addition of 0, 5, 10, or 50 μM TPEN (arrowheads). Insets show representative traces for eggs that
 949 resumed Ca²⁺ oscillations after TPEN. (C) As above, but following the addition of 100 μM EDTA, 100
 950 or 500 μM DTPA (time of addition denoted by arrowheads). (D) Ca²⁺ oscillations following ICSI after
 951 the addition of 50, 100, and 500 μM TPA (horizontal bars of increasing thickness). (E) Representative
 952 bright field images of ICSI fertilized eggs 2.5, 4, and 7 hr. after sperm injection. Arrows and
 953 arrowheads denote the second polar body and PN formation, respectively. Scale bar: 10 μm.

954 **Figure 2. TPEN dose-dependently inhibits Ca^{2+} oscillations in eggs triggered by a broad-**
 955 **spectrum of agonists that stimulate the PI pathway or IP₃R1.**



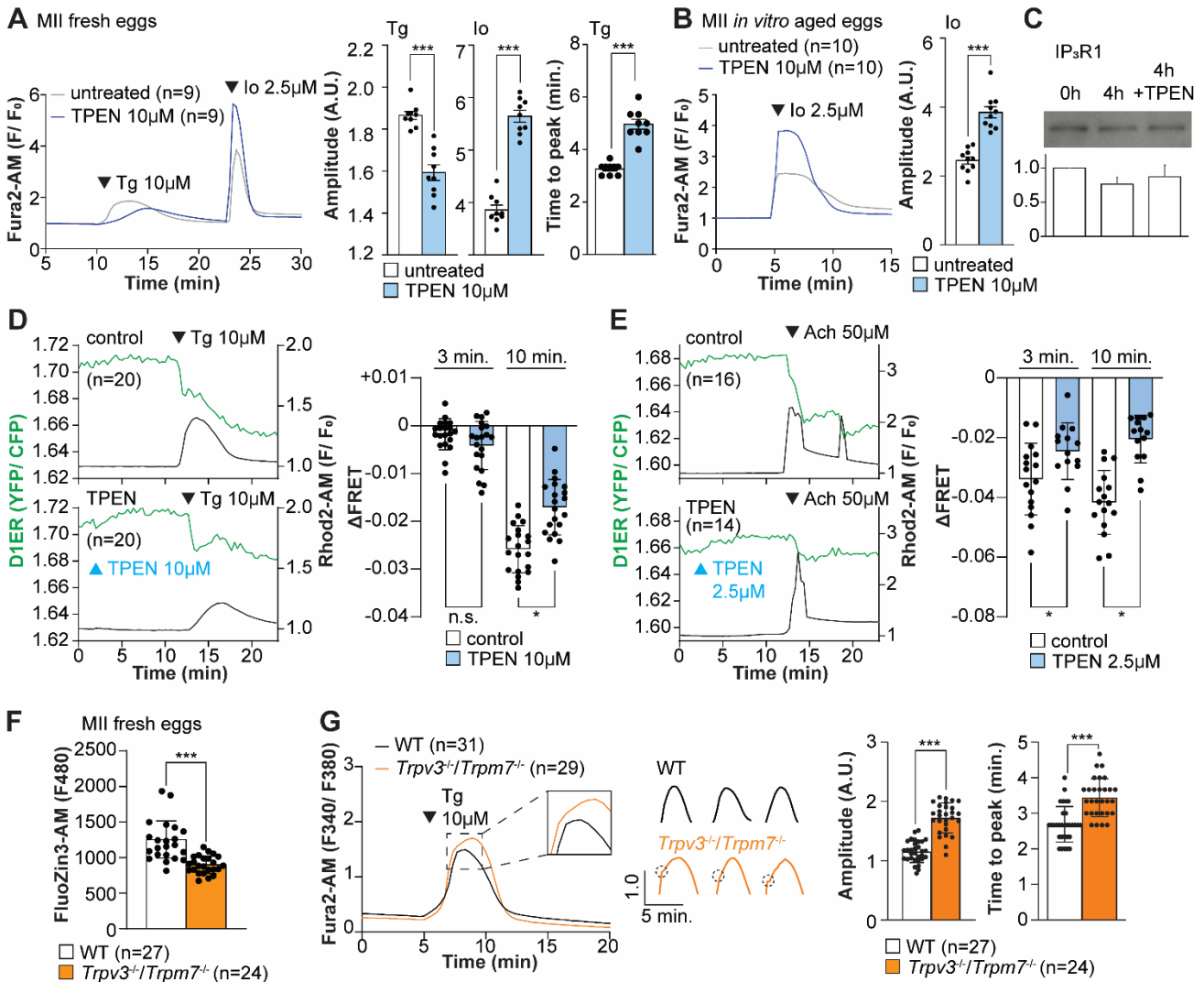
956
 957 (A-D) Representative Ca^{2+} responses induced by (A) *mPlcζ* mRNA microinjection (0.01 μg/μl, black
 958 traces), (B) strontium chloride (10 mM, green), (C) acetylcholine chloride (50 μM, orange), and (D)
 959 thimerosal (25 μM, purple) in MII eggs. Increasing concentrations of TPEN were added to the
 960 monitoring media (arrowheads above traces denotes the time of adding). Insets in the upper row show
 961 representative traces of eggs that stop oscillating despite others continuing to oscillate. (E) Each bar
 962 graph summarizes the TPEN effect on Ca^{2+} oscillations at the selected concentrations for each of the
 963 agonists in A-D. (F) Western blot showing the intensities of IP₃R1 and alpha-tubulin bands in MII eggs
 964 or in eggs injected with *mPlcζ* mRNA and incubated or not with TPEN above ($P < 0.01$). Thirty eggs
 965 per lane in all cases. This experiment was repeated twice, and the mean relative intensity of each blot
 966 is shown in the bar graph below.

967 **Figure 3. TPEN inhibition of cIP₃-induced Ca²⁺ release is precluded by ZnSO₄ supplementation**
 968 **before TPEN exposure.**



969
 970 (A-G) Representative Ca²⁺ responses in MII eggs triggered by the release of caged IP₃ (cIP₃) induced
 971 by UV light pulses of increasing duration (arrows). (A) A representative control trace without TPEN,
 972 and (B) following the addition of 10 μM TPEN between the third and the fourth pulses. The broken
 973 line rectangle is magnified in the inset, farthest right side of the panel displaying the near immediate
 974 termination of an ongoing rise. (C, D) Recordings started in the presence of 10 μM TPEN but in (D)
 975 100 μM ZnSO₄ was added between the second and the third pulses. (E) Recording started in the
 976 presence of 100 μM ZnSO₄ followed by the addition of 10 μM TPEN between the third and the fourth
 977 pulses. (F, G) Recording started in the presence of 100 μM MgSO₄ (F) or 100 μM CaCl₂ (G) and 10
 978 μM TPEN added as above. Arrowheads above the different panels indicate the time of TPEN or
 979 divalent cation addition. (H) Bar graphs summarizing the number and percentages of eggs that
 980 responded to a given duration of UV pulses under each of the TPEN±divalent ions.

981 **Figure 4. Zn²⁺ depletion alters Ca²⁺ homeostasis and increases Ca²⁺ store content independent of**
 982 **IP₃R1 mass.**

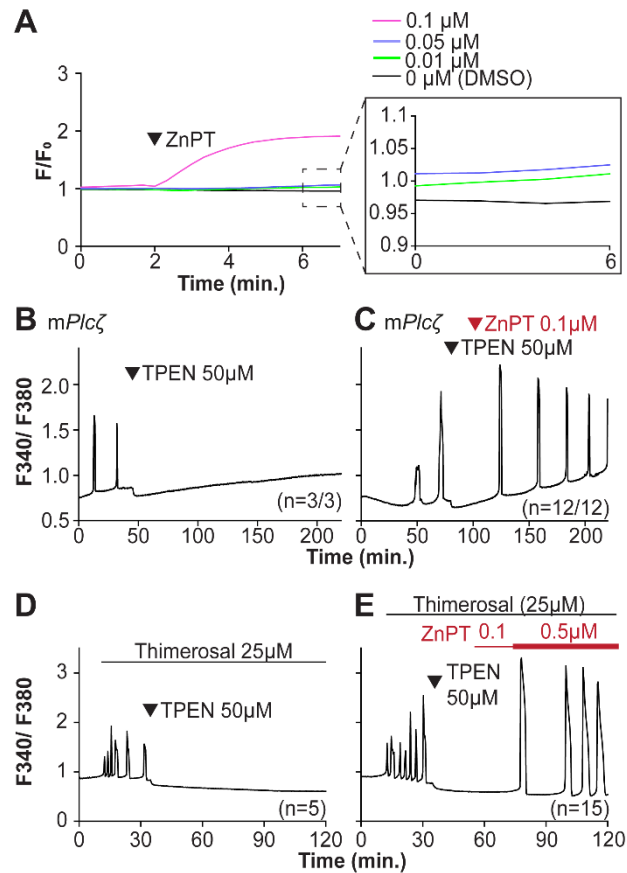


983

984 (A, B) Representative Ca²⁺ traces of MII eggs after the addition of Tg and Io in the presence or
 985 absence of TPEN. Blue trace recordings represent TPEN-treated eggs whereas gray traces represent
 986 control, untreated eggs. (A) Io was added to fresh MII eggs once Ca²⁺ returned to baseline after
 987 treatment with Tg. Comparisons of mean peak amplitudes after Tg and Io are shown in the bar
 988 graphs in the right panel ($P < 0.001$). (B) MII eggs were aged by 2-hr. incubation supplemented or
 989 not with TPEN followed by Io addition and Ca²⁺ monitoring ($P < 0.001$). (C) Western blot showing
 990 the intensities of IP₃R1 bands in MII eggs freshly collected, aged by 4-hr. incubation without TPEN,
 991 and with TPEN. Thirty eggs per lane in all cases. This experiment was repeated three times. (D, E)
 992 (Left panels) Representative traces of Ca²⁺ values in eggs loaded with the Ca²⁺-sensitive dye Rhod-2
 993 AM and the ER Ca²⁺ reporter, D1ER (1 μg/μl mRNA). TPEN was added into the media followed 10
 994 min. later by (D) 10 μM Tg and (E) 50 μM Ach. (Right panel) Bars represent the difference of FRET
 995 value between at the time of Tg/ Ach addition and at 3 and 5 min. later of the addition ($P < 0.05$).
 996 Experiments were repeated two different times for each treatment. Black and green traces represent

997 cytosolic Ca^{2+} and Ca^{2+} -ER, respectively. Blue and black arrowheads indicate the time of addition of
998 TPEN and Tg/ Ach, respectively. (F) Basal Zn^{2+} level comparison in WT (open bar) and *Trpv3*^{-/-}
999 /*Trpm7*^{-/-} (dKO, orange bar) MII eggs. Each plot represents the FluoZin3 measurement at 5 min. after
1000 starting monitoring. (G) (Left panel) Representative Ca^{2+} traces of WT (black trace) and dKO
1001 (orange trace) MII eggs after adding Tg. Insets represent the magnified traces at the peak of Ca^{2+}
1002 spike from different sets of eggs. (Middle panel) Individual traces of WT and dKO eggs after Tg
1003 addition. Dashed circles represent the flection point in dKO traces. (Right panel) Comparisons of
1004 mean peak amplitudes after Tg and the time between Tg addition and the Ca^{2+} peak are shown in the
1005 bar graphs in the right panel ($P < 0.001$)
1006

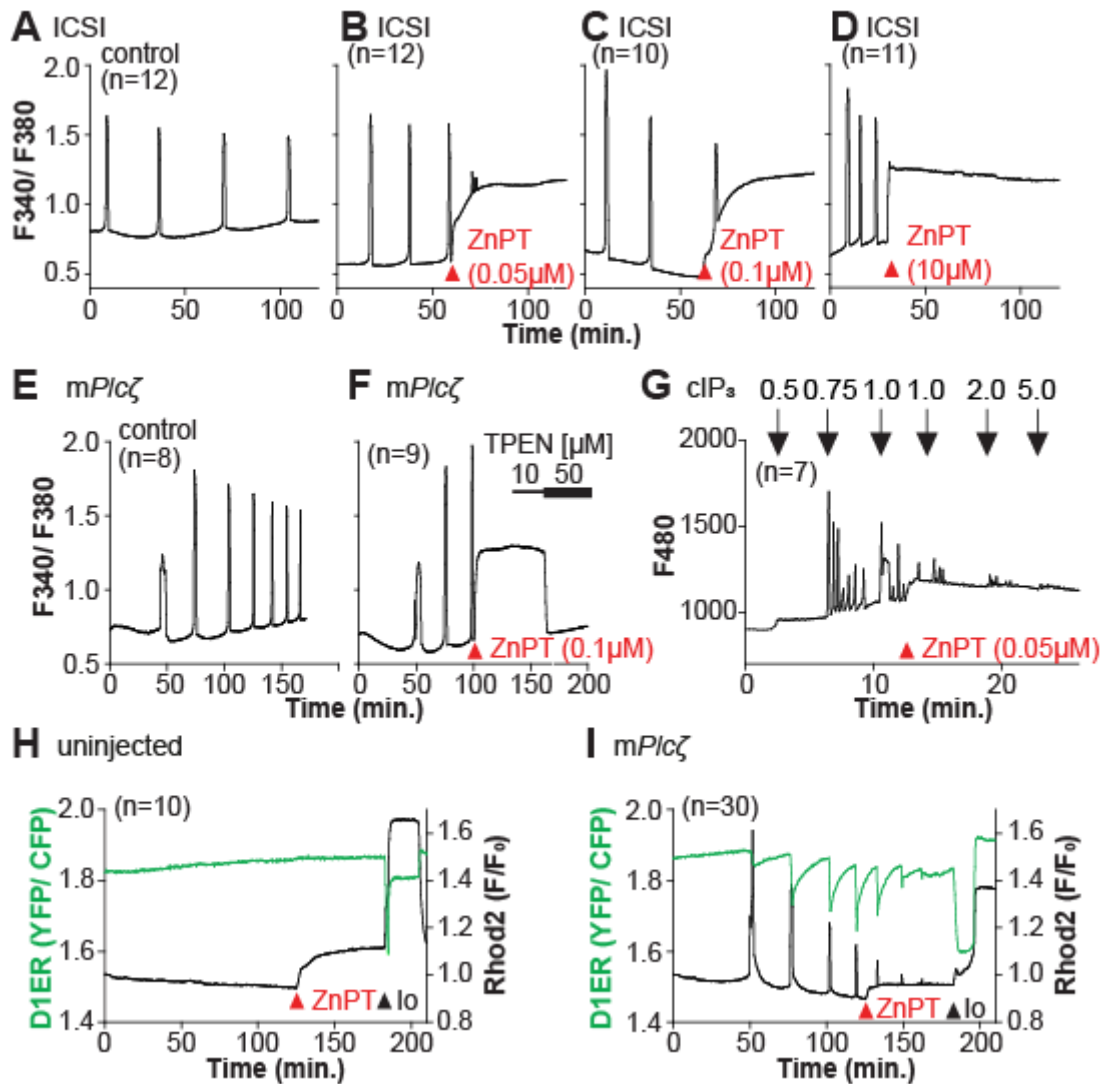
1007 **Figure 5. Restoring Zn^{2+} levels with ZnPT rescues oscillations interrupted by TPEN-induced**
1008 **Zn^{2+} deficiency.**



1009

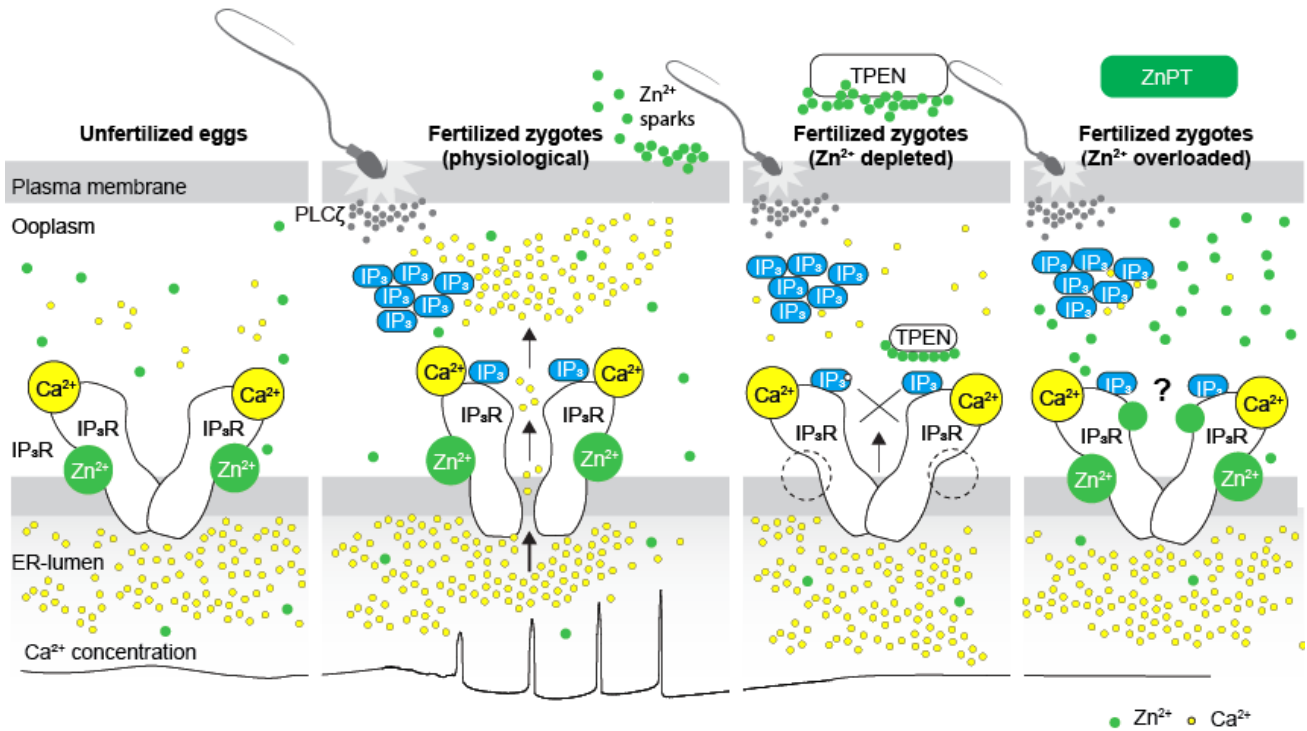
1010 (A) Representative traces of Zn^{2+} in MII eggs following the addition of 0.01 to 0.1 μM concentrations
1011 of ZnTP. The broken rectangular area is amplified in the next panel to appreciate the subtle increase in
1012 basal Zn^{2+} caused by the addition of ZnTP. (B, C) *mPlc ζ* mRNA (0.01 $\mu g/\mu l$)-induced oscillations
1013 followed by the addition of TPEN (black arrowhead) (B), or after the addition of TPEN followed by
1014 ZnPT (red arrowhead) (C). (D, E) Thimerosal (25 μM) induced oscillations using the same sequence
1015 of TPEN (D) and ZnPT (E), but higher concentrations of ZnPT were required to rescue Thimerosal-
1016 initiated oscillations (E). These experiments were repeated at least two different times.

1017 **Figure 6. Excess Zn²⁺ hinders Ca²⁺ oscillations.**



1018
 1019 (A-D) ICSI-initiated Ca²⁺ response without (A) or following the addition of ZnPT (B, C) (the time of
 1020 ZnPT addition and concentration are denoted above the tracing). (E, F) Representative Ca²⁺ responses
 1021 induced by injection of 0.01 μg/μl mPlcζ mRNA in untreated eggs (E) or in eggs treated with 0.1 μM
 1022 ZnPT followed by 10 μM TPEN first and then 50 μM (F). (G) cIP₃-induced Ca²⁺ release as expected
 1023 when the UV pulses in the absence but not in the presence of 0.05 μM ZnPT (the time of addition is
 1024 denoted by a bar above the tracing). (H, I) Representative traces of Ca²⁺ values in eggs loaded with the
 1025 Ca²⁺-sensitive dye Rhod-2 AM and the ER Ca²⁺ reporter, D1ER (1 μg/μl mRNA). Uninjected and 0.01
 1026 μg/μl mPlcζ mRNA-injected eggs were monitored. After initiation and establishment of the
 1027 oscillations, 0.1 μM ZnPT was added into the media followed 30 min later by 2.5 μM Io. Experiments
 1028 were repeated two different times. Red and black arrowheads indicate the time of addition of ZnPT
 1029 and Io, respectively.

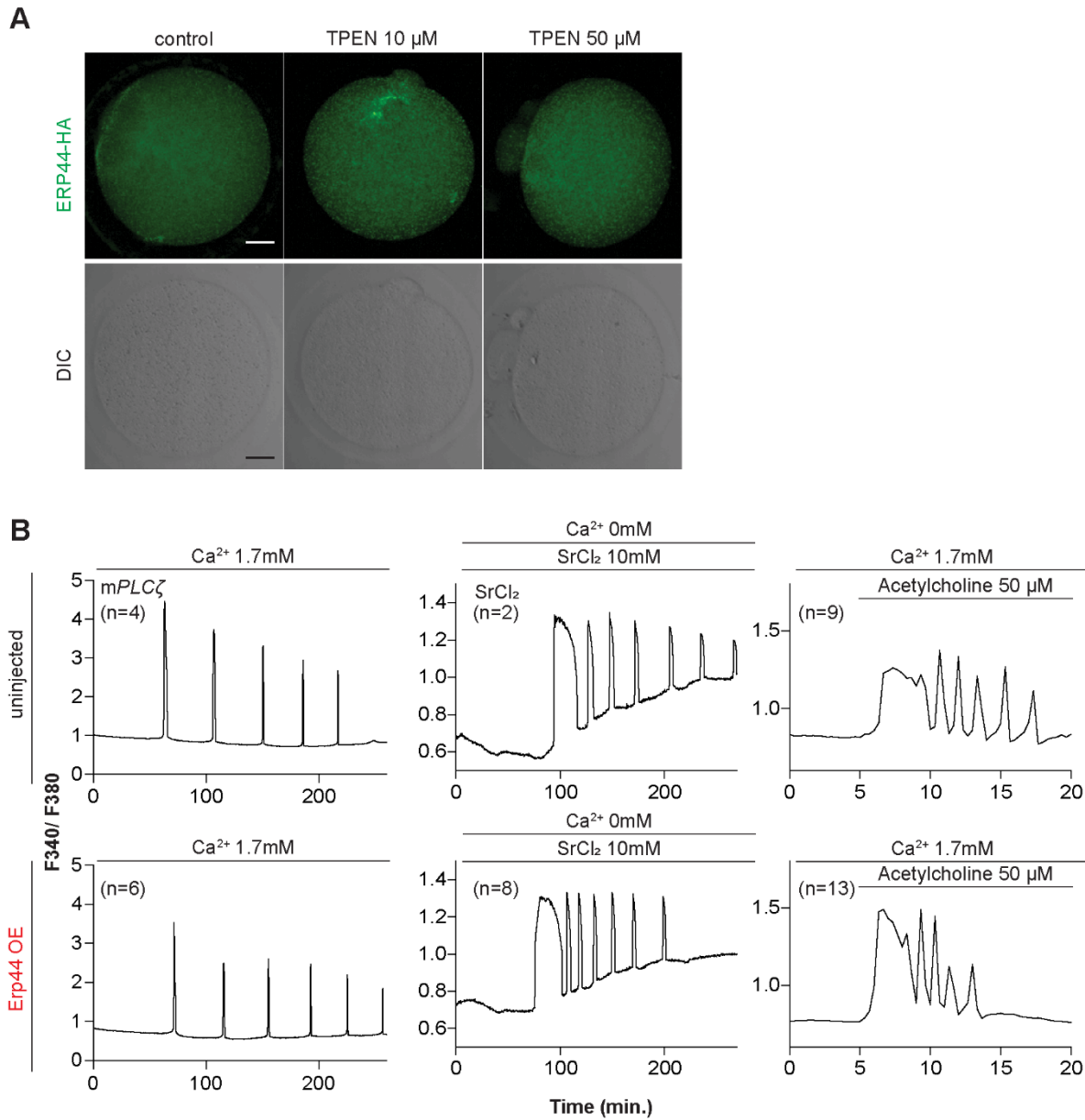
1030 **Figure 7. Schematic of proposed regulation of IP₃R1 function by Zn²⁺ in eggs and fertilized**
1031 **zygotes.**



1032

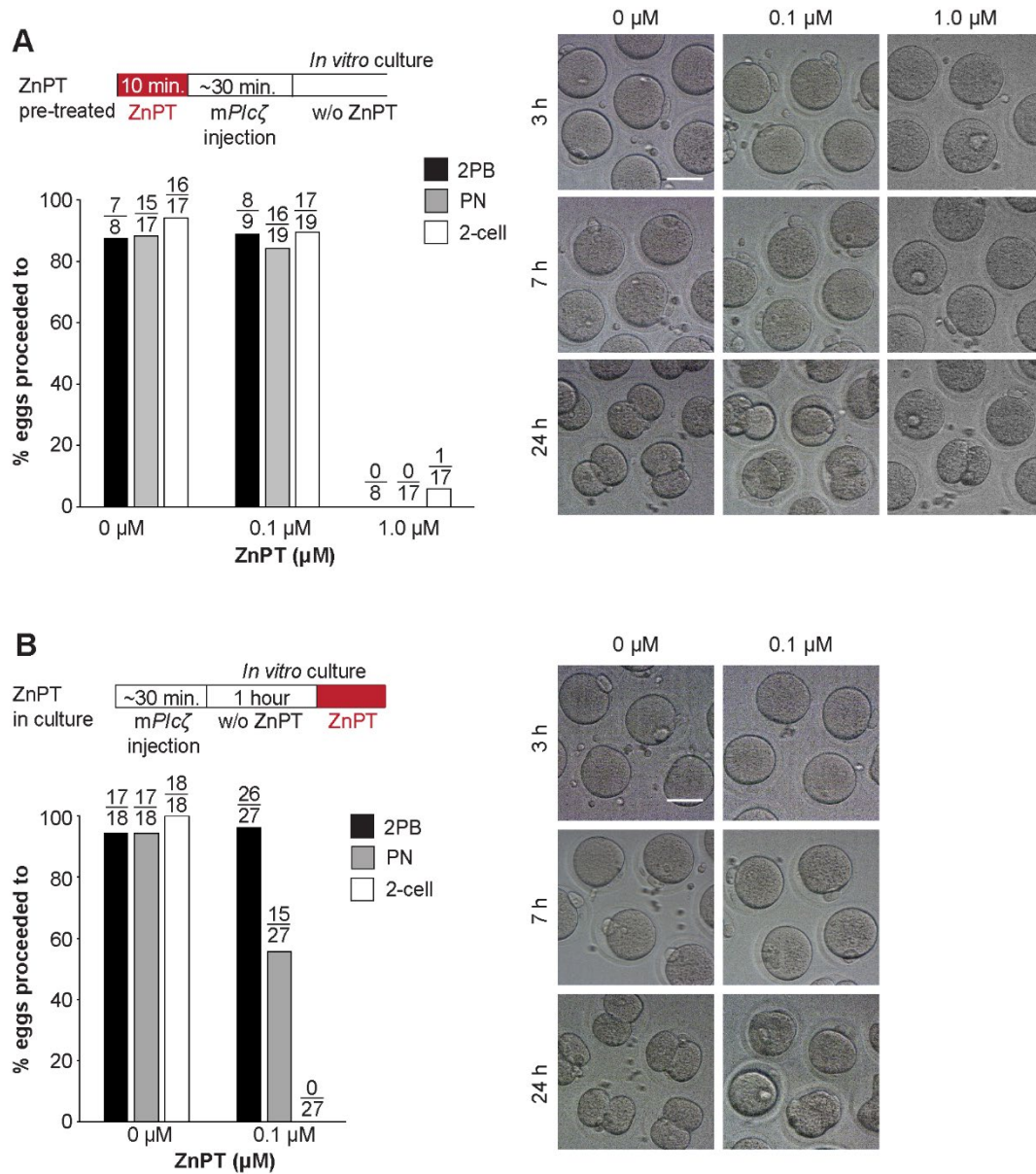
1033 In MII eggs, left panel, IP₃R1s are in a Ca²⁺-release permissive state with optimal levels of cytoplasmic
1034 Ca²⁺ and Zn²⁺ and maximum ER content, but Ca²⁺ is maintained at resting levels by the combined
1035 actions of pumps, ER Ca²⁺ leak, and reduced influx. Once fertilization takes place, left center panel,
1036 robust IP₃ production induced by the sperm-borne PLCζ leads to Ca²⁺ release through ligand-induced
1037 gating of IP₃R1. Continuous IP₃ production and refilling of the stores via Ca²⁺ influx ensure the
1038 persistence of the oscillations. Zn²⁺ release occurs in association with first few Ca²⁺ rises and cortical
1039 granule exocytosis, Zn²⁺ sparks, lowering Zn²⁺ levels but not sufficiently to inhibit IP₃R1 function.
1040 Zn²⁺ deficiency caused by TPEN or other permeable Zn²⁺ chelators, right center panel, dose-
1041 dependently impairs IP₃R1 function and limits Ca²⁺ release. We propose this is accomplished by
1042 stripping the Zn²⁺ bound to the residues of the zinc-finger motif in the LNK domain of IP₃R1 that
1043 prevents the allosteric modulation of the gating process induced by IP₃ or other agonists. We propose
1044 that excess Zn²⁺, right panel, also inhibits IP₃R1-mediated Ca²⁺ release, possibly by non-specific binding
1045 of thiol groups present in cysteine residues throughout the receptor (denoted by ?). We submit that
1046 optimal Ca²⁺ oscillations in mouse eggs unfold in the presence of a permissive range of
1047 Zn²⁺ concentration.

1048 **Supplementary Figure 1. Overexpression of ER accessory protein ERp44 did not change the Ca²⁺**
1049 **responses initiated by *mPlcζ* mRNA microinjection, Acetylcholine, or SrCl₂.**



1050
1051 (A) Representative immunofluorescent images of MII eggs with overexpression of ERp44. At 5 hr.
1052 post microinjection, eggs were treated with 10 or 50 μM of TPEN and incubated for 1 hr, after which
1053 they were fixed and stained. An anti-HA antibody was used. Scale bar: 10 μm. (B) Representative Ca²⁺
1054 responses induced by *mPlcζ* mRNA microinjection (0.01 μg/ μl-left column), SrCl₂ (10 mM-center
1055 column), and acetylcholine (50 μM-right column) in eggs with (top panels) or without (bottom panels)
1056 ERp44 overexpression.

1057 **Supplementary Figure 2. Elevated Zn²⁺ impairs egg activation and the subsequent embryo**
 1058 **development.**



1059

1060 (A) MII eggs were incubated in TL-HEPES containing 0, 0.1, or 1.0 μM ZnPT at room temperature
 1061 for 10 min and washed several times with fresh TL-HEPES and injected with *mP/cζ* mRNA. After it,
 1062 eggs and zygotes were cultured in KSOM for 24 hr. PN formation and 2-cell development were
 1063 checked at 7- and 24-hr post-microinjection. Bars represent the percentages of injected eggs that
 1064 reached the PN and the 2-cell stage. Scale bar: 50 μm. (B) MII eggs injected with *mP/cζ* mRNA were
 1065 incubated in KSOM without ZnPT for an hr. and then incubated in KSOM with 0 or 0.1 μM ZnPT for
 1066 24 hr. The second polar body extrusion, PN formation, and 2-cell development were checked at 2.5-,
 1067 7- and 24-hr. post-microinjection. Bars represent the percentages of injected eggs that reached the PN
 1068 and the 2-cell stage. Scale bar: 50 μm.